Porosity and Permeability Prediction through Forward Stratigraphic Simulations Using GPM™ and Petrel™: Application in Shallow Marine Depositional Settings.

Daniel Otoo and David Hodgetts

Department of Earth and Environmental Sciences, University of Manchester, Manchester, M13 9PL, United Kingdom.

Correspondence to: Daniel Otoo (daniel.otoo@manchester.ac.uk)

Abstract

The forward stratigraphic simulation approach was used to model porosity and permeability attributes in the Volve field, Norway. This was achieved by applying spatial data from the forward stratigraphic simulation to control property distribution in the reservoir model. Building a reservoir model that fits data at different locations is a task associated with high levels of uncertainty. To minimise property representation uncertainties in a reservoir model, geologically realistic sediment distribution patterns must be developed to predict lithofacies units and associated petrophysical properties. The workflow is in three parts; first, the geological process modeling (GPM™) software developed by Schlumberger was used to simulate scenarios of sediment transportation and deposition in the model area. Secondly, an estimation of lithofacies proportions in the stratigraphic model was done using the property calculator tool in the Petrel™ software. Finally, porosity and permeability values were assigned to corresponding lithofacies-associations in the forward model to produce a forward stratigraphic-based petrophysical model. Results show a lithofacies distribution that is controlled by sediment diffusion rate, sea level variation, flow rate, wave processes, and tectonic events. This observation is consistent with real-world events, were variation in sea level, volume of sediment input, and accommodation control the build-up of stratigraphic sequence. Validation wells, VP1 and VP2 located in the original Volve field petrophysical model and the forward stratigraphic-based models show a good match in porosity and permeability attributes at 5 m vertical sample intervals. The resultant forward stratigraphic-based porosity and permeability models suggests that forward stratigraphic simulation outputs can be integrated into classical modeling workflows to improve subsurface property representation, and well planning strategies.

Introduction

The distribution of reservoir properties such as porosity and permeability is a direct function of a complex combination of sedimentary, geochemical, and mechanical processes (Skalinski & Kenter, 2014). The impact of reservoir petrophysics on well planning and extraction strategies makes it imperative to use reservoir modeling techniques that present realistic property variations in 3-D models (Deutsch and Journel, 1999; Caers and Zhang, 2004; Hu & Chugunova, 2008). Typically, reservoir modeling require continued property modification until an a appropriate match to known subsurface data is obtained. However, acquisition of subsurface datasets is costly, thus restricts data collection and subsurface modeling conditions. Several studies, e.g. Hodgetts et al. (2004) and Orellana et al. (2014) have demonstrated that stratigraphic patterns, and therefore petrophysical attributes can be extrapolated from seismic, outcrop and well logs. However, this notion is limited by the absence of accurate and reliable 3-D depositional models to guide property modeling in reservoir units (Burges et al. 2008). Reservoir modeling techniques with the capacity to integrate forward stratigraphic simulation outputs with stochastic modeling techniques for subsurface property modeling will improve reservoir heterogeneity characterization, because they more accurately produce geological realism than the other modeling methods (Singh et al. 2013). The use of geostatistical-based methods to represent the spatial variability of reservoir properties have been widely accepted in many exploration and production projects (e.g. Kelkar and Godofredo, 2002). In geostatistical modeling methods, an alternate numerical 3-D model (i.e. realizations) is derived to demonstrate different scenarios of property distribution that can be conditioned to well data (Ringrose & Bentley, 2015). Reservoir modeling practioners are normally faced with the challenge of getting a lot of subsurface data to deduce reliable variogram models as a result of cost, therefore introducing a significant level of uncertainty in a reservoir model (Orellena et al. 2014). The advantages of applying geostatistical approaches in populating propoerties in reservoir models is well established (e.g. Deutsch and Journel, 1999; Dubrule, 1998), but the geostatistical-based method tends to confine reservoir property models to known data and rarely realize geological realism to capture sedimentary that have led to reservoir formation (Hassanpour et al. 2013). In effect, the geostatistical

modeling technique is unable to reproduce a long-range continuous reservoir properties that are essential for generating realistic reservoir connectivity models (Strebelle & Levy, 2008). Based on lessons from a previous work (e.g. Otoo and Hodgetts, 2019), the forward stratigraphic simulation approach was applied in this contribution to predict lithofacies units, porosity, and permeability properties in a 3-D model. An important aspect of this work is the use of variogram parameters from forward stratigraphic-based synthetic wells to populate petrophysical properties in the reservoir model grid. Forward stratigraphic modeling involves the uses morphodynamic rules to derive sedimentary depositional trends to reflect stratigraphic patterns in known data. The approach is driven by the principle that multiple sedimentary process-based simulations in a 3-D framework will improve facies, and petrophysical property distribution in a geological model.

The reservoir interval under study is located within the Hugin formation. Studies by Varadi et al. (1998); Kieft et al. (2011), suggest that the formation consist of a complex depositional architecture of waves, tidal and fluvial processes. This indicates that a single depositional model will not be adequate to produce a realisitc lithofacies distributions model of the area. Furthermore, the complicated Syn-depositional rift-related faulting system, significantly influence the stratigraphic architecture (Milner and Olsen, 1998). The focus of this work is to produce a depositional sequence in the shallow marine environment by using a forward stratigraphic modeling approach in the GPM^{TM} (Schlumberger, 2017), and use variogram parameters from the forward model to control porosity and permeability property representation in the Volve field model grid.

Study Area

The Volve field (Figure 1), located in Block 15/9 south of the Norwegian North Sea is Jurassic in age (i.e. late Bajocian to Oxfordian) with the Hugin Formation as the main reservoir unit from which hydrocarbons are produced (Vollset and Dore, 1984). The Hugin formation is made up of shallow marine to marginal marine sandstone deposits, coals, and a significant influence of wave events that tend to control lithofacies distribution in the formation (Varadi et al. 1998; and Kieft et al. 2011). Several studies, e.g. Sneider et al. (1995), and Husmo et al. (2003) associate sediment deposition in the Hugin system to

a rift-related subsidence and successive flooding during a large transgression of the Viking Graben within the Middle to Late Jurassic period. Previously it was interpreted to comprise of marine shoreface, lagoonal and associated coastal plain, back-stepping delta-plain and delta front deposits (e.g. Cockings et al. 1992; Milner and Olsen, 1998), but recent studies, e.g. Folkestad and Satur, (2006) suggest the influence of a strong tidal event, which introduces another dimension in property modeling of the reservoir. The thickness of the Hugin formation is estimated to range between 5 m and 200 m but can be thicker off-structure and non-existent on structurally high segments as a result of post-depositional erosion (Folkestad and Satur, 2006).

Based on studies by Kieft et al. (2011), a summarised sedimentological delineation within the Hugin formation is presented in **Table 1**. Lithofacies-association codes A, B, C, D, and E used in the classification represents bay fill units, shoreface sandstone facies, mouth bar units, fluvio-tidal channel fill sediments, and coastal plain facies units respectively. In addition a lithofacies association prefixed code F was interpreted to consist of open marine shale units, mudstone with occasional siltstone beds, parallel laminated soft sediment deformation that locally develop at bed tops. The lateral extent of the code F lithofacies package in the Hugin formation is estimated to be 1.7 km to 37.6 km, but the total thickness of code F lithofacies is not known (Folkestad & Satur, 2006).

Data and Software

This work is based on description, and interpretation of petrophysical datasets in the Volve field by Statoil, now Equinor. Datasets include 3-D seismic sections, and a suite of 24 wells that consist of formation pressure data, core data, and sedimentological logs. Previous works such as Folkestad & Satur, (2006) and Kieft et al. (2011) show varying grain size, sorting, sedimentary structures, bounding contacts of sediment matrix that play a significant part of the reservoir petrophysics. Grain size, sediment matrix and the degree of sorting will typically drive the volume of void created, and therefore the porosity and permeability attributes . Wireline-log attributes such as gamma ray (GR), sonic (DT), density (RHOB), and neutron-porosity (NPHI) were used to distinguish lithofacies units, stratigraphic horizons and zones that are required to build the 3-D property model. Porosity, and permeability models, of the Volve field,

were generated in Schlumberger's Petrel™ software. Importantly, this work also seeks to produce geologically realistic depositional architecture that is comparable to a real-world stratigraphic framework in a shallow marine environment. Deriving a representative 3-D stratigraphic model of the reservoir allows us to deduce geometrical and variogram parameters as input datasets in actual subsurface property modeling.

Schlumberger's geological process modeling (GPM™) software was used to undertake twenty forward stratigraphic simulation in an attempt to replicate depositional processes that resulted in the build-up of the reservoir interval under study. Simulations were constrained to twenty scenarios because the desired stratigraphic sequence and associated sediment patterns were achieved at the fourth simulation. The main criteria for evaluating the realistic nature of a stratigraphic model was to compare it to the depositional sequence observed in the seismic section in Figure 3b. Several process modeling software packages exist and have been applied in similar studies; e.g. Delft3D-Flow™; Rijin & Walstra, (2003); DIONISOS™; Burges et al. (2008). The geological process modeling (GPM™) software was preferred because of the availability of software license, and also the ease in integrating of its outputs into the property modeling workflow in Petrel™.

Methodology

The workflow **(**Figure 2a) combines the stratigraphic simulation capacity of the GPM™ software in different depositional settings, and the property modeling tools in Petrel™ to predict the distribution of porosity and permeability properties away from well data. Three broad steps have been used here to achieve this goal; (i) forward stratigraphic simulation (FSS) in GPM™ software (2019.1 version), (ii) lithofacies classification using the calculator tool in Petrel™, and (iii) lithofacies, porosity, and permeability modeling in Petrel™ (2019.1 version).

Process Modeling in GPM™

The GPM™ software consist of different geological processes that are designed to replicate sediment deposition in clastic and carbonate environments. For example, previous studies, e.g. Kieft et al, (2011)

identified the influence of riverine (fluvial), and wave processes in the genetic structure of sediments in the Hugin formation. These geological processes could be very rapid depending on accommodation generated as a result of sea level variation, and or sediment composition and flow intensity. Sediment deposition, and its response to post-depositional sedimentary and tectonic processes are significant in the ultimate distribution of subsurface lithofacies units. To attain stratigraphic outputs that fall within the depositional architecture captured in the seismic section (Figure 3b), the input parameters were varied as illustrated by different scenarios in Table 2. The simulation generated geologically realistic stratigraphic trends, but also revealed some limitations, such as instability in the simulator when more than three geological processes and sub-operations run at a time. In view of this, the diffusion and tectonic processes were combined with other processes such as steady flow, unsteady flow, and sediment accumulation to replicate the Volve field stratigraphic depositional scenarios.

Steady Flow Process

The steady flow process in GPM simulate flows that changes slowly over a period, or sediment transport scenarios where flow velocity and channel depth do not vary abruptly; e.g. rivers at normal stage, deltas, and sea currents. The steady flow process can be specified to a desired setting in the "run sedimentary simulation" dialog box in the Petrel^{TM} software (version 2017.1 and above). Considering the influence of fluvial activities in the build-up of the Hugin formation, it was important to capture its impact on the resultant simulated output. To attain stability in the simulator, it is advisable to undertake preliminary runs to ascertain the appropriateness of input parameters that will be used in the simulation. For steady flow process, a boundary condition must be specified at the edges of the model. For example in an open flow system, negative integers (i.e. values below zero) must be assigned to the edges of the hypothetical paleo-surface to allow water to enter and leave the simulation area.

Unsteady Flow Process

The unsteady flow process can model flows that are periodic, and run for a limited time; for example, in turbidites where velocity of flow and depth changes abruptly over time. The unsteady flow process algorithm is set up to apply a number of fluid elements, that are affected by gravity, and by friction against

the hypothetical topographic surface. A contribution on the application of the unsteady in stratigraphic simulation, and how its settings can be configured to attain geological realistic outcomes is discussed in Otoo and Hodgetts, (2019).

Diffusion Process

The diffusion process can effectively replicate sediment erosion from areas of higher slope (i.e. source location) and their deposition to lower elevation of the model area. Sediment dispersion in the diffusion process is carried out through erosion and transportation processes that are driven by gravity in the simulator. The diffusion process is based on the assumption that sediments are transported downslope at a proportional rate to the topographic gradient; therefore making fine grained sediments easily transportable than coarse grained sediments. Diffusion is controlled by two parameters; (i) diffusion coefficient, which controls the strength of the diffusion, and (ii) diffusion curve that serves as a unitless multiplier in the algorithm. The governing equation for the diffusion process is:

$\frac{\partial z}{\partial t} = k\nabla^2 z$, where **z** is topographic elevation, **k** the diffusion coefficient, **t** for time, and $\nabla^2 z$ is the laplacian.

Sediment Accumulation

In the GPM^{TM} software, sediment source can be set to a point location or considered to emanate from a whole area. Sediment accumulation deals with sediment deposition via an areal source. For example, where a lithology is interpreted to be uniformly distributed, the sediment accumulation process can be used to replicate such depositional scenario. The areal input rates for each sediment type (e.g. coarse grained, fine grained sediments) used in the accumulation process must be specified in the settings. Specifying the areal rates for each sediment is important because the software is configured to use the value of the surface at each cell in the model grid and multiplies it by a value (i.e. value from a unitless curve) at each time step in the simulation to estimate the thickness of sediments accumulated or eroded from a cell in the model.

Parameters for Forward Stratigraphic Simulation

A realistic reproduction of stratigraphic patterns in the study area will require input parameters or initial conditions such as: hypothetical paleo-topography, sea level curves, sediment source location and distribution curve, tectonic event maps (i.e. subsidence and uplift), and sediment mix velocity. The application of these input parameters in GPM^{TM}, and their influence on the resultant stratigraphic framework are discussed below.

Hypothetical Paleo-Surface: The hypothetical paleo-topographic surface, on which the simulation evolves was inferred from the seismic section. This is done with the assumption that the present day stratigraphic surface (i.e. paleo shoreline in Figure 3a) occurred as a result of basin filling through different geological periods. Since the hypothetical topography generated from the seismic section have undergone various phases of subsidence and uplifts, the paleo topographic surface used in this work does not present an accurate description of the basin at the period of sediment deposition. To obtain an appropriate paleo-topographic for this task, , five paleo topographic surfaces (TPr) were generated by adding or subtracting elevations from the inferred paleo topographic surface (see Figure 4g) using the equation: TPr = Sbs + EM, where, Sbs is the base surface scenario (in this instance, scenario 6), and EM an elevation below and above the base surface. Paleo-topographic surface in scenario 3 (figure 4d) was selected, because it controlled the development of stratigraphic sequences that fit the conceptual knowledge of depositional framework as observed in the seismic section (Figure 5d).

Sediment Source Location: Based on regional well correlations in previous studies (e.g. Kieft et al. 2011), and seismic interpretation of the basin structure, the sediment entry point was placed in the north-eastern section of the hypothetical paleo-topography. Since the exact sediment entry point is not known, multiple entry points were placed at 4 km radius around the primary location in (Figure 3c), in order to capture possible sediment source locations. The source position is characterised by positive integers (i.e. values greater than zero) to enable fluid flow to other parts of the simulation surface.

Sea Level: Sea level variation was inferred from published studies and facies description in shallow marine depositional environments (e.g. Winterer and Bosellini, 1981). To attain stability in the simulator, we assumed a sea level that range between 15 m to 45 m; averaging 30 m for short simulation runs, e.g. 5000 to 20000 years. The sea level was varied with increasing duration of the simulation (illustrated in Table 2). The peak sea-level in the simulation represents the maximum flooding surface (Figure 5d), and therefore the inferred sequence boundary in the geological process model.

Diffusion and Tectonic Event Rates: The sediment mix proportion, diffusion rate and tectonic event functions were inferred from previous studies (e.g. Walter, 1978; Winterer and Bosellini, 1981, and Burges et al., 2008). The diffusion and tectonic event rates are increased or reduced to produce a stratigraphic model that fit our knowledge of the basin evolution. A key criteria for selecting parameters is their capacity to produce stratigraphic outputs that depict depositional scenarios in the study area. For example, in scenario 1 (Figure 6a), the early stages of clinoform development show resemblance to interpreted trends in the seismic section (Figure 3b). As a result, input figures that were higher and lesser than those used in generating scenario 1 were generated to serve as the simulation parameters for the twenty scenarios. In scenario 1, a diffusion coefficient of 8 m2/a was used to produce a realistic clinoform build-up, so the figure was varied with +/- 5 to obtain figures that could improve the model derived in scenario 1. The initial topography (TP_r) was kept constant throughout a simulation, but wave events, steady/unsteady flow, diffusion and tectonic events use curve functions to provide variations within the simulation. A sudden change in subsidence rate tends to constrain coarse to medium sediments at proximal distance to source location than in scenarios where the rate of subsidence was made gradual.

The influence of input parameters in the simulation is evident whenever there is a slight change of value in sediment diffusion, and tectonic rates or dimension of the hypothetical topographic surfaces. For example, sediment source position has a strong impact on the extent and depth to which sediments are deposited in the basin. Shifting the source point to the mid-section of the topography (i.e. the mid-point of the topography in a basin-ward direction) resulted in the accumulation of distal elements that are identical to turbidite lobe systems. This is consistent with morphodynamic experiments by de Leeuw et al., 2016, where sediment discharge from the basin slope leads to the build-up of basin floor fan units.

Property Classification in Stratigraphic Model

In our opinion, the most appropriate model in this work is **Figure 5d**. This is because, when compared to depositional description in studies such as Folkestad and Satur (2006); kieft et al., (2011), it produced a stratigraphic sequence that mimics the depositional sequence in the study area. The stratigraphic model was converted into a 3-D format, 20 m x 20 m x 2 m grid cells in order to be used in the property modeling tool in Petrel^{TM}. Lithofacies, porosity, and permeability properties are characterized in the stratigraphic using a rule based approach (**Table 3**). Sediment distribution in each time step of the simulation were stacked into a single zone framework to attain a simplified model. This was done with the assumption that sedimentary processes that lead to the final build-up of genetic related units within zones of the model will not vary significantly over the simulation period. Property classification in the model was achieved with the property calculator tool in Petrel^{TM}. The classification was driven by depositional depth, geologic flow velocity, and sediment distribution patterns as indicated in **Figure 7**. Lithofacies representation in the stratigraphic model was based on the sediment grain size pattern, and proximity to sediment source. For example, shoreface lithofacies units were characterized using medium-to-coarse grained sediments, which accumulate at proximal distance to the sediment source. In contrast, mudstone units were restricted to fine grained sediments that accumulate at distal section of the simulation domain.

Using published studies by Kieft et al., (2011), porosity and permeability variations in the stratigraphic model were estimated from wireline-log attributes such as gamma ray, neutron, sonic, and density logs outlined in Table 1. In previous studies on the Sleipner Øst, and Volve field (e.g. Equinor, 2006; Kieft et al., 2011), Shoreface deposits were identified to make up the best reservoir units, whilst lagoonal deposits formed the worst reservoir units. Using this as guide, shoreface sandstone units and mudstone/shale units in the forward stratigraphic model were characterized as best and worst reservoir units respectively. The porosity and permeability values in Table 4 were derived from equations in Statoil's petrophysical report of the Volve field (Equinor, 2016):

$\emptyset_{er} = \emptyset_D + \alpha \,.\, (NPHI - \emptyset_D) + \beta;$ where $\emptyset_{er}$ is the estimated porosity range, $\emptyset_D$ is density porosity, α and β are regression constants; ranging between -0.02 – 0.01 and 0.28 – 0.4 respectively, *NPHI* is neutron

porosity. In instances where NPHI values for lithofacies units is not available from the published references, an average of 0.25 was used.

$KLOGH_{er} = 10^{(2 + 8 * PHIF - 5 * VSH)}$; where $KLOGH_{er}$ is the estimated permeability range, *VSH* is the volume of clay/shale in the lithofacies unit, and *PHIF*, the fractured porosity. The *VSH* range between 0.01 – 0.12 for the shoreface units, and 0.78 – 0.88 for lagoonal deposits.

Property Modeling in Petrel™

The workflow (**Figure 2b**) used for subsurface property (e.g. lithofacies, and petrophysical) modeling in Petrel™ is extended to represent lithofacies, porosity, and permeability properties in the forward stratigraphic model. These processes include:

1. Structure modelling: identified faults within the study area are modelled together with interpreted surfaces from seismic and well data to generate the main structural framework, within which the entire property model will be built. The procedures involve modification of fault pillars and connecting fault bodies to one another to attain the kind of fault framework interpreted from seismic and core data.

(2) Pillar gridding: a "grid skeleton" that is made up of a top, middle and base architectures. Typically, pillars join corresponding corners of every grid cell of the adjacent grid to form the foundation for each cell within the model. The prominent orientation of faults (i.e. I-direction) within the model area generally trends in a N-S and NE-SW direction, so the "I-direction" was set to the NNE-SSW direction to capture the structural description.

(3) Horizons, Zones and Vertical Layering: stratigraphic horizons and subdivisions (zones) delineates the geological formation's boundaries. As stratigraphic horizons are inserted into the model grid, the surfaces are trimmed iteratively and modified along faults to correspond with displacements across multiple faults. Vertical layering on the other hand defines the thicknesses and orientation between the layers of the model. Layers in this context describes significant changes in particle size or sediment composition in a geological formation. Using a vertical layering scheme makes it possible to honour the fault framework, pillar grid and horizons that have been derived. A

constant cell thicknesses of 1 m across the model was defined to control the vertical scale, in which subsurface properties such as lithofacies, porosity, and permeability attributes are modelled.

(4) Upscaling: involves the substation of fine grid cells with coarser grid cells. This is done to assign property values to cells in order to evaluate which discrete value suits each a selected data point. One advantage of the upscaling procedure is to make the modeling process faster.

Porosity and Permeability Modeling

The porosity and permeability model that was built by Equinor for their operations in the Volve field was adopted as the base model. The model, which cover an area of 17.9 km^2 was generated with the reservoir management software (RMS), developed by Irap and Roxar (Emerson^{TM}). The petrophysical model has a grid dimension of 108 m x 100 m x 63 m, and was compressed by 75.27% of cell size from an approximated cell size 143 m x 133 m x 84 m. To achieve a comparable model resolution as the Volve field porosity and permeability model, the forward stratigraphic output, which had an initial resolution of 90 m x 78 m x 45 m was upscaled to a grid of 107 m x 99 m x 63 m. Two options were explored with respect to the use of variogram parameters derived from forward model-based synthetic wells. Option 1 was to assign porosity and permeability values to the synthetic lithofacies wells that correspond to known facies-associations as indicated in **Table 4**. The synthetic wells with porosity and permeability data are placed in-between known data locations to guide porosity and permeability property distribution in the model. For option 2, the best-fit forward stratigraphic model was populated with porosity, and permeability attributes using the major stratigraphic orientation captured in the seismic data (i.e. NE-SW; 240º) to control property distribution trends. Porosity and permeability were populated into the model by using the property modeling process in Petrel^{TM}. Porosity and permeability synthetic logs are then extracted from the forward stratigraphic output to build the porosity and permeability models (**Figure 8**). Taking into account the possibility that vertical trends in options 1 and 2 will be similar in a sampled interval, it is our opinion that option 2 will provide a viable 3-D representation of property variations in the major and minor directions of the forward stratigraphic model. Ten synthetic wells (SW), ranging between 80 m and a 120 m in total depth (TD) were positioned in the forward model to capture the vertical distribution of porosity-permeability at different sections of the stratigraphic model.

The forward-based synthetic wells (**Figure 9 c**) with porosity and permeability logs were upscaled to populate the original structural model using the sequential Gaussian simulation method. Here, the synthetic wells derived from the stratigraphic model is to provide an additional well data for use in a traditional modeling workflow as was the case in the building of original Volve model. Considering the advantages of variogram-based modeling in relation to data conditioning, the idea was to get more wells into the model grid to control porosity and permeability distribution. Upscaling the synthetic well data in this context is to "transform" the data from 1-D into a 3-D framework to build the property model. Using the same structural model was to attain a comparable framework for evaluating the modeling outputs.

The variogram model (**Figure 10**), of dominant lithofacies units in the formation served as a guide in the estimation of variogram parameters from the forward model. A major and minor range of 1400 m and 400 m respectively, and an average sill value of 0.75 derived from forward stratigraphic-based synthetic wells were used to populate porosity and permeability properties in the model. Porosity models were derived with a normal distribution, whilst the permeability models were produced using a log-normal distribution and the corresponding porosity property for collocated co-kriging. Out of fifty model realizations, six realizations that showed some similarity to the original petrophysical model are presented (**Figure 11**). This was accomplished through visual and statistical comparison of zones in the original Volve field model, and the stratigraphic-based porosity/permeability models. The statistical approach involved a comparison of summary statistics from the original Volve model, and the porosity/permeability model generated through forward stratigraphic modeling. The visual comparison on the other hand looked at how geological realistic the output is, and if it conforms with our conceptual idea of the Volve field model.

Results

The stratigraphic model in stage 4 (**Figure 5d iv**) shows the final geometry after 700, 000 years of simulation time. Initial simulation produced a progradation sequence with foreset-like features (**Figure 5d i**). A sequence boundary, which indicates the highest sea level in the model separates the initial simulated output from the next prograding phase (**Figure 5d ii**). Initiation of an aggradation stacking

pattern starts, and becomes prominent in stage 3 (**Figure 5d iii**). These sequences are consistent with real-world scenario where sediment supply matchup with accommodation created as a result of the relative sea level rise within a period (e.g. Muto and Steel, 2000; Neal and Abreu, 2009). The diffusion process in GPM^{TM} was used to define the stratigraphic architecture before introducing additional geological processes such as steady flow, unsteady flow, wave events to capture the range of possible depositional styles that have been discussed in published literature (e.g. Folkestad & Satur, 2006; Kieft et al., 2011).

The impact of the stratigraphic simulation on porosity and permeability representation in the model was evaluated by comparing its outcomes to the Volve field porosity and permeability models by using two synthetic well, VP1 and VP2, which were sampled vertically at a 5 m intervals. Considering that the Volve field petrophysical model (**Figure 11a**) have undergone phases of history matching to enhance well planning, and production strategies in the Volve field, it is reasonable to assume that porosity and permeability distribution in the petrophysical model will be geologically realistic and less uncertain. A good match in porosity was observed in validation wells that penetrate the model realizations; R14, R20, R26, R36, R45, and R49 (**Table 5a**). Figure 12 shows the porosity variation (0.18 – 0.24) in some selected realizations**.** This value (i.e. 0.18 – 0.24) is within the range of porosity estimates in the Volve field (Equinor, 2016). In view of the limitation in making variations within a simulation run in GPM^{TM}, the forward stratigraphic-based model (FSM) was derived with an assumption that variogram parameters, stratigraphic inclination within zones will remain constant. As a result, the original petrophysical model, which involve other measured attributes within the stratigraphic zone was not considered in the forward stratigraphic modeling-based permeability model, hence the major variations noted in **Table 5b.** Typically, a petrophysical model like the Sleipner Øst and Volve field model will take into account other sources of data. For example, data from a special core analysis (SCAL) will improve the reservoir petrophysics assessment. Considering that the FSM approach did not involve these additional information from the formation, it is reasonable to suggest that the forward stratigraphic-based porosity and permeability models have been adequately conditioned to known subsurface data.

Discussion

Results show the influence of sediment transport rate, (or diffusion rate), initial basin topography and sediment source location on stratigraphic simulation in the GPM^{TM} software. Similar to other studies (e.g. Muto & Steel, 2000; Neal & Abreu, 2009), a variations in sea level controls the volume of sediment that could be retained or transported further into the basin; therefore controlling the kind of stratigraphic sequences that are generated. In a related work by Burges et al. (2008), it was established that a sediment-wedge topset width was directly linked to the initial bathymetry, in which the sediment-wedge structure was formed, as well as the correlation between sediment supply and accommodation rate. This is in line with observations in this study, where the initial sediment deposit control the geometry of subsequent phase of depositions. The uncertainty of initial conditions used in this work led to the generation of multiple forward stratigraphic scenarios to account for the range of bathymetries that may have influenced sediment transportation to form the present day Hugin formation. The simulation produced well defined sloping depositional surfaces in a stratigraphic architecture (i.e. clinoforms) and sequence boundaries that depict the pattern observed in the seismic data. Indicated in previous studies, (e.g. Allen and Posamentier, 1993; Ghandour and Haredy, 2019) sequence stratigraphy is vital in the characterization of lithofacies in sedimentary systems. Therefore, a reproduction of stratigraphic sequence in 3-D, using the forward stratigraphic modeling approach in GPM^{TM} provide a good framework to analyse property variations in a reservoir. A porosity-permeability model matching the original petrophysical model was produced using synthetic porosity and permeability logs from the forward stratigraphic model as input datasets in the sequential Gaussian simulation algorithm. As mentioned previously, this exercise did not take into account variations in the layering scheme that develops in different zones of the stratigraphic model. Under this circumstance, we concede that there is a possibility to overestimate and or underestimate porosity and permeability properties as observed in some sampled intervals of the validation wells. In view of this, it is our suggestion that forward stratigraphic simulation outputs should be applied as additional data to understand sediment distribution patterns, and associated vertical and horizontal petrophysical trends in the depositional environment than using its outputs as an absolute conditioning data in subsurface property modeling.

Assumptions made with respect to the type of geological processes, and input parameters to use in the simulation certainly differ from what existed during the period of deposition. So, applying stratigraphic models that fit a basin scale description to a smaller scale reservoir context presents another degree of uncertainty in the approach used here. For example, in their study, Burges et al., (2008) shows that the diffusion geological process fits the description of large scale sediment transportation; suggesting that an extrapolation of its outputs into a well-scale framework could produce results that deviate from the real world distribution. In reality, sediment deposition into a geological basin is also controlled by mechanical and geochemical processes that tend to modify a formations petrophysical attributes (Warrlich et al. 2010). Therefore, using different geological processes and initial conditions to generate depositional scenarios is a reasonable approach. However, based on the approach limitation, which are also discussed in similar works (e.g. . Bertoncello et al. 2013; Aas et al. 2014; and Huang et al. 2015) caution must be taken in using its outputs in real reservoir modeling; as it could lead to an increase in property representation bias.

The correlation between reservoir lithofacies and petrophysics have been examined in previous studies, e.g. Falivene et al. (2006) Hu and Chugunova, (2008), but the difference in predicted and actual reservoir character is less understood. This in large part is due to the absence of a realistic 3-D stratigraphic framework to guide reservoir property representation in geocellular models. It is our opinion that forward stratigraphic modeling methods provide reservoir modeling practitioners a better platform to generate appropriate 3-D lithofacies models to improve petrophysical property prediction in a reservoir, but its outputs should be used cautiously and together with verifiable subsurface patterns from seismic and well datasets.

Conclusion

In this paper, spatial data from a forward stratigraphic simulation is combined with subsurface data from the Volve field, Norway to constrain porosity and permeability distribution in inter-well regions of the model area. As caution, the forward stratigraphic simulation scenarios presented in this contribution do not ultimately prove that spatial and geometrical data derived from stratigraphic modeling can be used as

absolute input parameters for a real-world reservoir modeling task. Uncertainties in the choice of initial condition and processes for the stratigraphic simulation led the variation of input parameters in order to attain a depositional architecture that is geologically realistic and comparable to the stratigraphic correlation suggested in some published studies of the study area. The good match obtained from validation wells in the original and stratigraphic-based petrophysical model, leads us to the suggestion that an integration of variogram parameters from well data and forward stratigraphic simulation outputs will improve property prediction in inter-well zones. This suggestion is supported by the idea that more conditioning data (well data) will increase the chance of producing realistic property distribution in the model area. In addition, this work also made some key findings:

1. For a specific application of forward stratigraphic modeling in GPM^{TM} and a range of model parameters, the process of sediment deposition is influenced by diffusion rate, and proximity to sediment source. This is consistent with several published works on sequence stacking and or system tracts in shallow marine settings, but further work with different stratigraphic modeling simulators could be useful in mitigating some of the challenges faced in this work.
2. A geologically viable 3-D lithofacies distribution in the shallow marine Hugin formation was achieved, which is evident in scenarios where sediment distribution vertically matches with lithofacies variation in a sampled interval in an actual well log.

Geologically feasible stratigraphic patterns generated in the forward stratigraphic model provide additional confidence in the representation of lithofacies, and therefore porosity and permeability property variations in the depositional setting under study. The resultant forward stratigraphic-based porosity and permeability model suggests that forward stratigraphic simulation outputs can be integrated into classical modeling workflows to improve subsurface property modeling , and well planning strategies.

Data and Code Availability

The datasets used in this work was obtained from Equinor on their Volve field operations, Norway. This include: 24 suits of well logs, and 3-D reservoir models in Eclipse and RMS formats. The data, models (eclipse and RMS formats), and the rule-based calculation script to generate lithofacies and porosity/permeability proportions are archived on Zenodo as Otoo & Hodgetts, (2020).

GPM™ Software

The version (2019.1) of GPM™ software was used in completing this work after an initial 2018.1 version. Available on: https://www.software.slb.com/products/gpm. The software license and code used in the GPM™ cannot be provided, because Schlumberger does not allow the code for its software to be shared in publications.

Model Availability in Petrel™

Petrel™ software (2017.1) was initially used for the task, but completed with Petrel™ software (2019.1); available on: https://www.software.slb.com/products/petrel. The software run on a windows PC with the following specifications: Processor; Intel Xeon CPU E5-1620 v3 @3.5GHz 4 cores-8 threads, Memory; 64 GB RAM. The computer should be high end, because a lot of processing time is required to execute a task. The forward stratigraphic models are achieved in Zenodo as Otoo & Hodgetts, (2020).

Author Contribution

Daniel Otoo designed the model workflow, conducted the simulation using the GPM™ software, and evaluated the results. David Hodgetts converted the Volve field data into Petrel compactible format for easy integration with outputs from the stratigraphic simulation.

Acknowledgement

Thanks to Equinor for making available the Volve field dataset. Also, thanks to Schlumberger for providing us with the GPM™ software license. A special thanks to Schlumberger for providing the software, and Mostfa Legri (Schlumberger) for his technical support in the use of GPM™. Finally, to the Ghana National Petroleum Corporation (GNPC) for sponsoring this research.

References

Aas, T., Basani, R., Howell, J. & Hansen, E.: Forward modeling as a method for predicting the distribution of deep-marine sands: an example from the Peira Cava sub-basin. The geologic society, 387(1), 247-269, doi:10.1144/SP387.9, 2014.

Allen, G. P. and Posamentier, H. W.: Sequence stratigraphy and facies model of an incised valley fill; the Gironde Estuary, France. Journal of Sedimentary Research; 63 (3), 378–391, doi:/10.1306/D4267B09-2B26-11D7-8648000102C1865D, 1993.

Bertoncello, A., Sun, T., Li, H., Mariethoz, G., & Caers, J.: Conditioning Surface-Based Geological Models to Well and Thickness Data. International Association of Mathematical Geoscience, 45, 873-893, doi: 10.1007/s11004-013-9455-4, 2013.

Burges, P.M., Steel, R.J., & Granjeon, D.: Stratigraphic Forward Modeling of Basin-Margin Clinoform Systems: Implications for Controls on Topset and Shelf Width and Timing of Formation of Shelf-Edge deltas. Recent advances in models of siliciclastic shallow-marine stratigraphy. SEPM (Society for Sedimentary Geology) Special Publication, vol. 90, SEPM (Society for Sedimentary Geology), 35-45, 2008.

Caers, J., & Zhang, T.: Multiple-point geostatistics: a quantitative vehicle for integrating geologic analogs into multiple reservoir models, in Grammer, G. M., Harris, P. M., and Eberli, G. P., eds., Integration of outcrop and modern analogs in reservoir modeling. Am. Assoc. Petrol. Geol. Memoir, 384–394, 2004.

Cockings, J.H., Kessler, L.G., Mazza, T.A., & Riley, L.A.: Bathonian to mid-Oxfordian Sequence Stratigraphy of the South Viking Graben, North Sea. Geological Society, London, Special publications, 67, 65–105, doi:10.1144/GSL.SP.1992.067.01.04, 1992.

Deutsch, C. & Journel, A.: GSLIB. Geostatistical software library and user's guide. Geological magazine, 136(1), 83-108, doi:10.2307/1270548, 1999.

De Leeuw, J., Eggenhuisen, J.T., & Cartigny, M.J.B.: Morphodynamics of submarine channel inception revealed by new experimental approach. Nature Communication, 7, 10886, 2016.

Dubrule, O.: Geostatistics in Petroleum Geology. American Association of Petroleum Geologist, 38, 27-101, doi:10.1306/CE3823, 1998.

Falivene, O., Arbues, P., Gardiner, A., & Pickup, G.E.: Best practice stochastic facies modeling from a channel-fill turbidite sandstone analog (the Quarry outcrop, Eocene Ainsa basin, northeast Spain. American Association of Petroleum Geologist, 90(7), 1003-1029, doi:10.1306/02070605112, 2006.

Folkestad, A., & Satur, N.: Regressive and transgressive cycles in a rift-basin: Depositional model and sedimentary partitioning of the Middle Jurassic Hugin Formation, Southern Viking Graben, North Sea. Sedimentary Geology. 207, 1-21, doi:10.1016/j.sedgeo.2008.03.006, 2008.

Ghandour, I.M. and Haredy, R.A.: Facies Analysis and Sequence Stratigraphy of Al-Kharrar Lagoon Coastal Sediments, Rabigh Area, Saudi Arabia: Impact of Sea-Level and Climate Changes on Coastal Evolution. Arabian Journal for Science and Engineering, 44(1), 505-520, 2019.

Hassanpour, M., Pyrcz, M. & Deutsch, C.: Improved geostatistical models of inclined heterolithic strata for McMurray formation, Canada. AAPG Bulletin, 97(7), 1209-1224, doi:10.1306/01021312054, 2013.

Hodgetts, D.D., Drinkwater, N.D., Hodgson, J., Kavanagh, J., Flint, S.S., Keogh, K.J. and Howell, J.A.: Three-dimensional geological models from outcrop data using digital data collection techniques: an example from the Tanqua Karoo depocenter, South Africa. Geological Society, London, v. 171 (4), 57–75, doi:10.1144/GSL.SP.2004.239.01.05, 2004.

Hu, L.Y., and Chugunova, T.: Multiple-point geostatistics for modeling subsurface heterogeneity: A comprehensive review. Water Resource Research, 44 (11), 1-14, doi:10.1029/2008WR006993, 2008.

Huang, X., Griffiths, C. & Liu, J.: Recent development in stratigraphic forward modeling and its application in petroleum exploration. Australian journal of Earth science, 62(8), 903-919, doi:10.1080/081200991125389, 2015.

Husmo, T. & Hamar, G.P. & Høiland, O. & Johannessen, E.P. & Rømuld, A. & Spencer, A.M. & Titterton, Rosemary.: Lower and Middle Jurassic. In: The Millennium Atlas: Petroleum Geology of the Central and Northern North Sea, 129-155, 2003.

Kelkar, M., & Perez, G.: Applied Geostatistics for Reservoir Characterization. Society of Petroleum Engineers. https://www.academia.edu/36293900/Applied Geostatistics for Reservoir characterization. Accessed 10 September, 2019, 2002.

Kieft, R.L., Jackson, C.A.-L., Hampson, G.J., and Larsen, E.: Sedimentology and sequence stratigraphy of the Hugin Formation, Quadrant 15, Norwegian sector, South Viking Graben. Geology Society, London, Petroleum Geology Conference Series, 7, 157-176, doi:10.1144/0070157, 2011.

Milner, P.S., and Olsen, T.: Predicted distribution of the Hugin Formation reservoir interval in the Sleipner Øst field, South Viking Graben; the testing of a three-dimensional sequence stratigraphic model. In: Gradstein, F.M., Sandvik, K.O., Milton, N.J. (Eds.), Sequence Stratigraphy; Concepts and Applications. Special Publication, Vol 8. Norwegian Petroleum Society, 337-354, 1998.

Muto, T., and Steel, R.J.: The accommodation concept in sequence stratigraphy: Some dimensional problems and possible redefinition. Geology, 130(1), 1-10, 2000.

Neal, J., and Abreu, V.: Sequence stratigraphy hierarchy and the accommodation succession method. Geology, 37(9), 779-782, 2009.

Otoo, D., and Hodgetts, D.: Geological Process Simulation in 3-D Lithofacies Modeling: Application in a Basin Floor Fan Setting. Bulletin of Canadian Petroleum Geology, 67(4), 255-272, 2019.

Otoo, D. & Hodgetts, D. Data citation for a forward stratigraphic-based porosity and permeability model developed for the Volve field, Norway. Dataset. Zenodo. http://doi.org/10.5281/zenodo.3855293, 2020.

Orellana, N. Cavero, J. Yemez, I. Singh, V. and Sotomayor, J.: Influence of variograms in 3D reservoir-modeling outcomes: An example. The leading edge, 33(8), 890-902, doi:10.1190/tle33080890.1, 2014.

Patruno, S., and Hansen, W.H.: Clinoforms and clinoform systems: Review and dynamic classification scheme for shorelines, subaqueous deltas, shelf edges and continental margins. Earth-Science Reviews, 185, 202-233, 2018.

Ravasi, M., Vasconcelos, I., Curtis, A. and Kristi, A.: Vector-acoustic reverse time migration of Volve ocean-bottom cable data set without up/down decomposed wavefields. Geophysics 80 (4): 137-150, doi:10.1190/geo2014-0554.1, 2015.

Ringrose., P. & Bentley., M.: Reservoir model design: A practioner's guide. First edition ed. New York: Springer business media B.V. 20-150, 2015.

Rijn, L.C., Walstra, D.J.R., Grasmeijer, B., Sutherland, J., Pan, S., & Sierra, J.P.: The predictability of cross-shore bed evolution of sandy beaches at the time scale of storms and seasons using process-based profile models. Coastal engineering, 47(3), 295-327, doi:10.1016/S0378-3839(02)00120-5, 2003.

Schlumberger™ Softwares.: Geological Process Modeling, Petrel™ version 2019.1, Schlumberger, Norway. URL: https://www.sdc.oilfield.slb.com/SIS/downloads.aspx, 2019.

Singh, V., & Yemez, I., & Sotomayor de la Serna, J.: Integrated 3D reservoir interpretation and modeling: Lessons learned and proposed solutions. The Leading Edge. 32(11), 1340-1353, doi:10.1190/tle32111340.1, 2013.

Skalinski, M., & Kenter, J.: Carbonate petrophysical rock typing: Integrating geological attributes and petrophysical properties while linking with dynamic behaviour. Geological Society, London, Special Publications. 406 (1), 229-259, 2014.

Sneider, J.S., de Clarens, P., and Vail, P.R.: Sequence stratigraphy of the Middle and Upper Jurassic, Viking Graben, North Sea. In: Steel, R.J., Felt, V.L., Johannessen, E.P., Mathieu, C. (Eds.), Sequence Stratigraphy on the Northwest European Margin. Special Publication, vol. 5. Norwegian Petroleum Society, 167–198, doi:10.1016/S0928-8937(06)80068-8, 1995.

Statoil, "Sleipner Øst, Volve Model, Hugin and Skagerrak Formation Petrophysical Evaluation, 2006", Stavanger, Norway. Accessed on: April, 27, 2019. Online: https://www.equinor.com/volve-field-data-village-download.

Strebelle, S., & Levy, M.: Using multiple-point statistics to build geologically realistic reservoir models: the MPS/FDM workflow. Geological Society London, special publication, 309, 67-74, doi:10.1144/SP309.5, 2008.

Varadi, M., Antonsen, P., Eien, M., & Hager, K.: Jurasic genetic sequence stratigraphy of the Norwegian block 15/5 area, South Viking Graben. In: Gradstein, F. M., Sandvik, K.O., & Milton, N.J., (eds) Sequence Stratigraphy – Concepts and Applications. Norwegian Petroleum Society, Trondheim, special publication, 373-401, 1998.

Vollset, J. and Dore, A.G.: A revised Triassic and Jurassic lithostratigraphic nomenclature for the Norwegian North Sea. NPD Bulletin Oljedirektoratet, 3, 53, 1984.

Walter C. P.: Relationship between eustacy and stratigraphic sequences of passive margins. GSA Bulletin; 89 (9), 1389–1403, 1978.

Winterer, L. W., Bosellini, A.: Subsidence and Sedimentation on Jurassic Passive Continental Margin, Southern Alps, Italy. AAPG Bulletin; 65 (3), 394–421, doi: 10.1306/2F9197E2-16CE-11D7-8645000102C1865D, 1981.

Warrlich, G., Hillgartner, H., Rameil, N., Gittins, J., Mahruqi, I., Johnson, T., Alexander, D., Wassing, B., Steenwinkel, M., & Droste, H.: Reservoir characterisation of data-poor fields with regional analogues: a case study from the Lower Shuaiba in the Sultanate of Oman, p. 577, 2010.

List of Figures

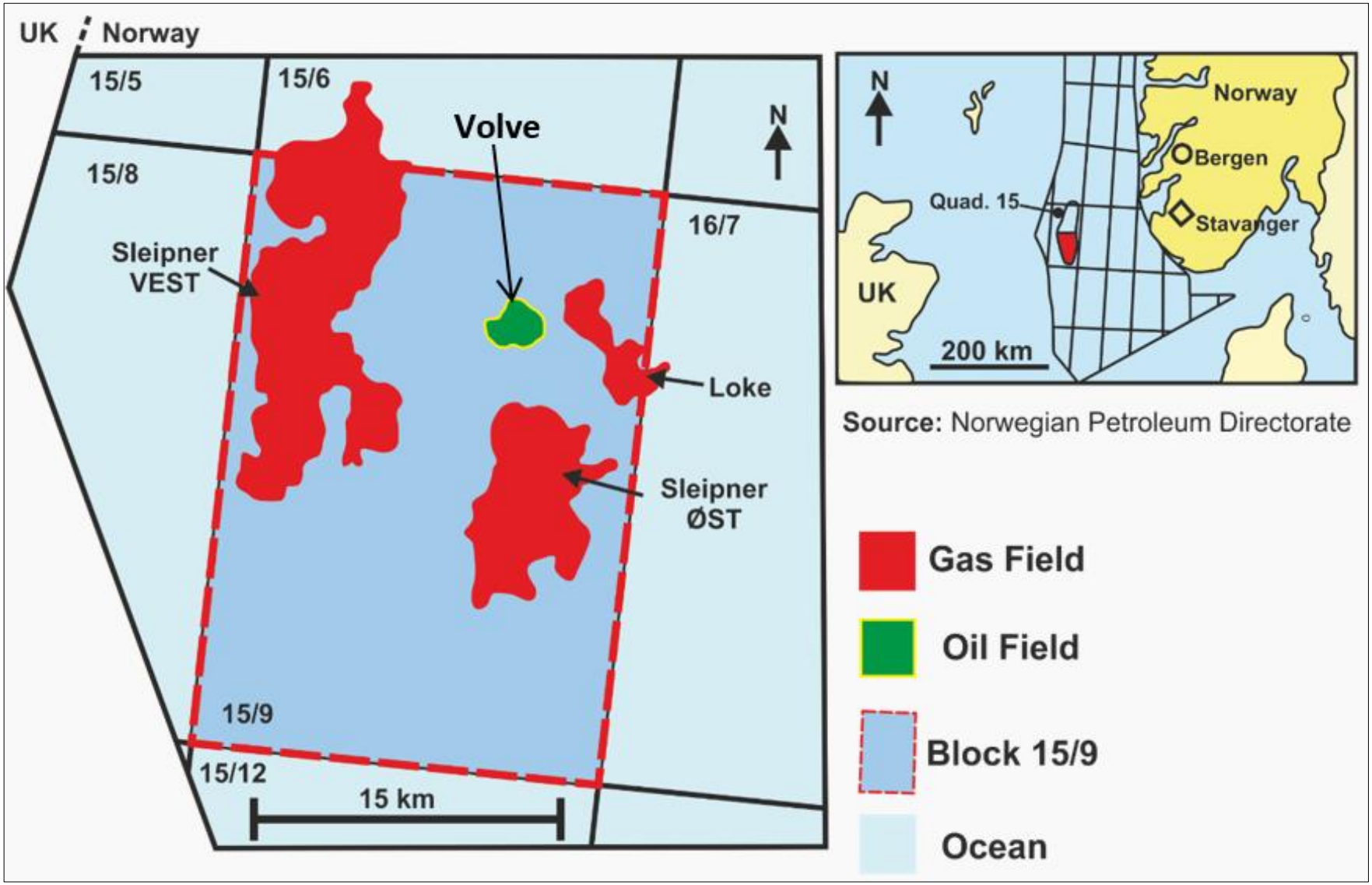

Fig 1. Location map of the Volve field, showing gas and oil fields in quadrant 15/9, Norwegian North Sea (Adapted from Ravasi et al., 2015).

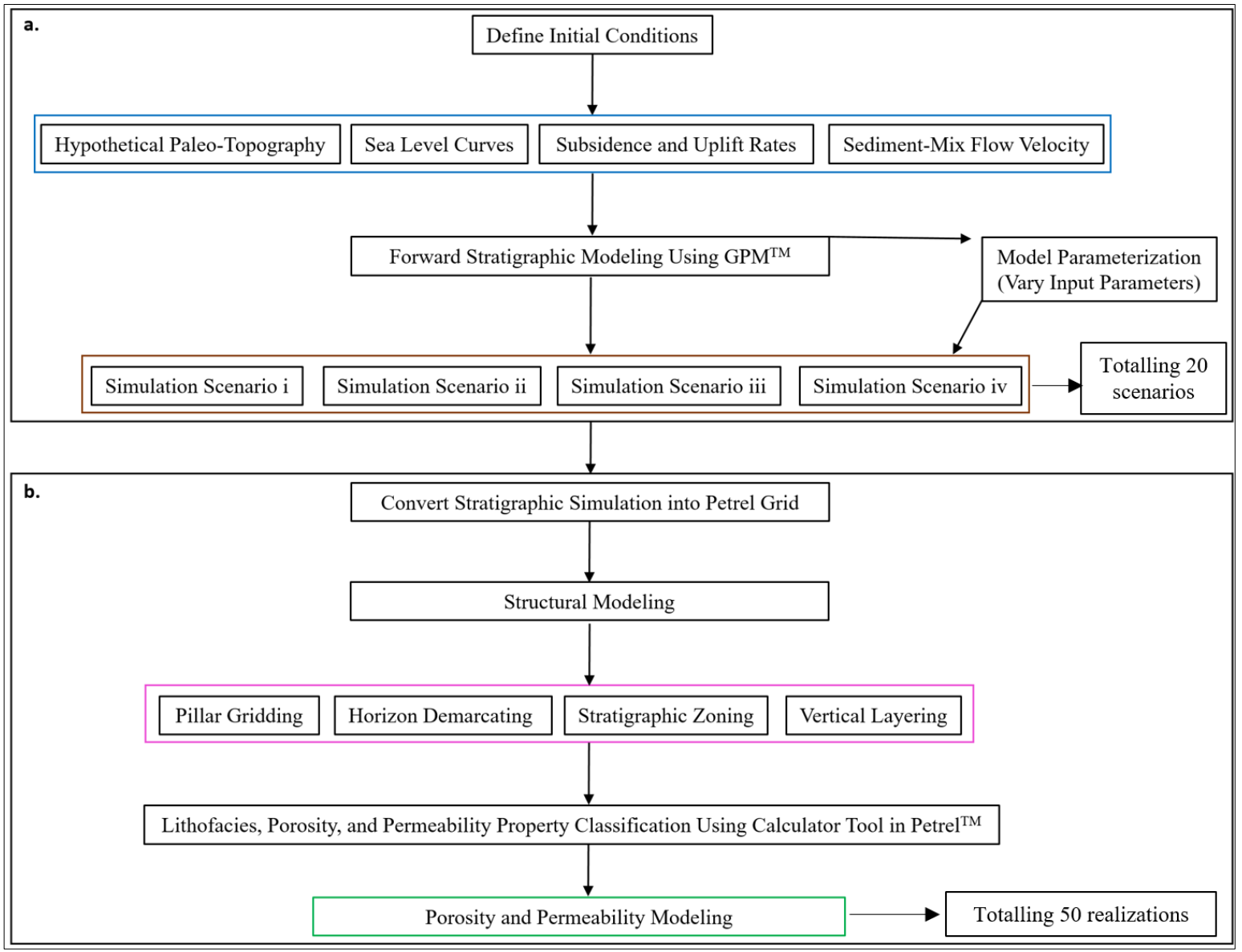

Fig 2. Schematic workflow of processes involved this work. a. providing information of initial conditions (or input parameters) that were used in the forward stratigraphic simulation in GPM™, b. demonstrating how the forward stratigraphic were converted into a grid that is usable in Petrel™ for porosity and permeability modeling.

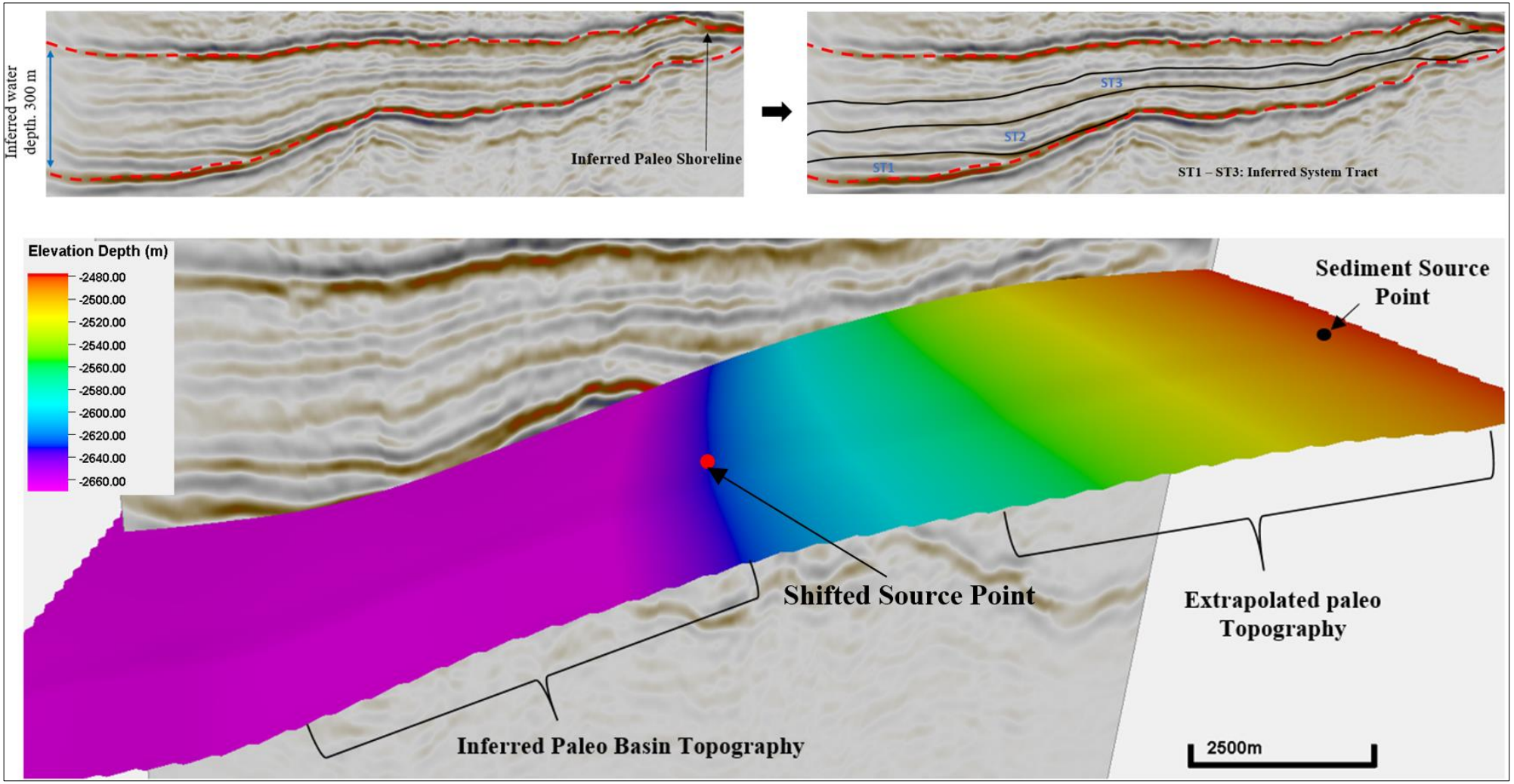

Fig 3. 3-D seismic section of the study area, from which the hypothetical topographic surface was derived for the simulation. The sedimentary entry point into the basin is located in the North Eastern section, based on previous study in the model area (e.g. Kieft et al. 2011).

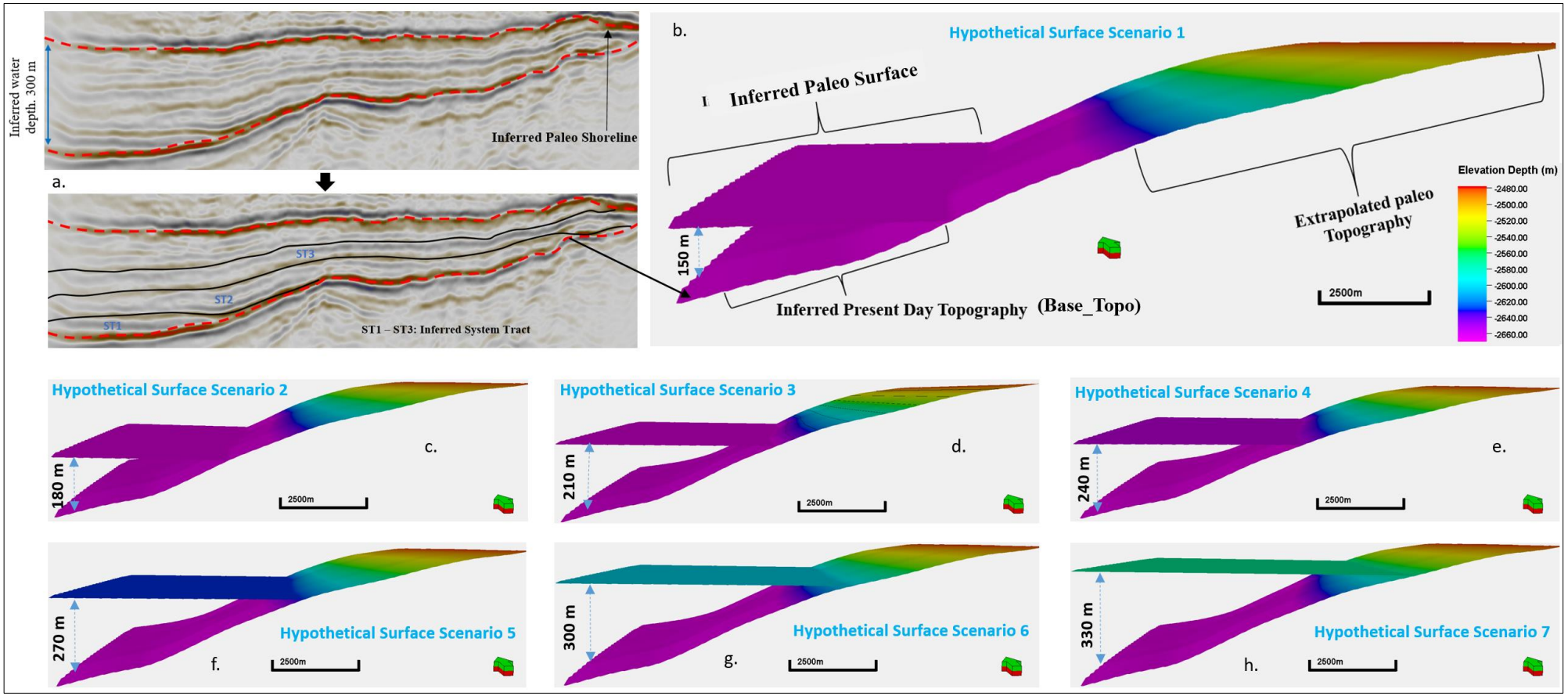

Fig 4. Inferred paleo topographic surface from seismic, also illustrating different topographic surface scenarios used in the simulation.

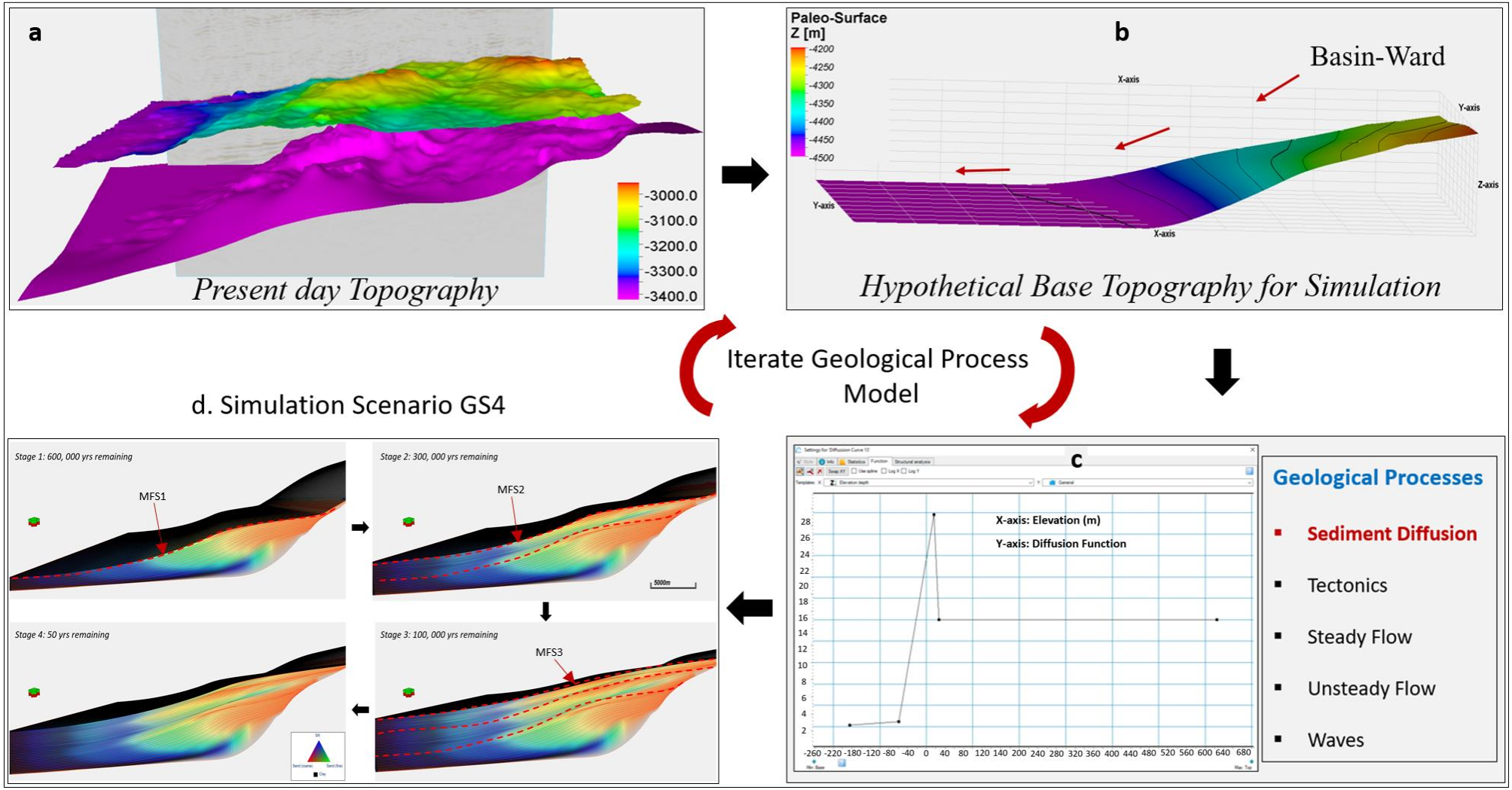

Fig 5. a. present day top and bottom topographic surfaces of the Hugin formation; b. hypothetical topographic surface derived from seismic data; c. geological processes involved in the simulation; d. forward stratigraphic models at different simulation time.

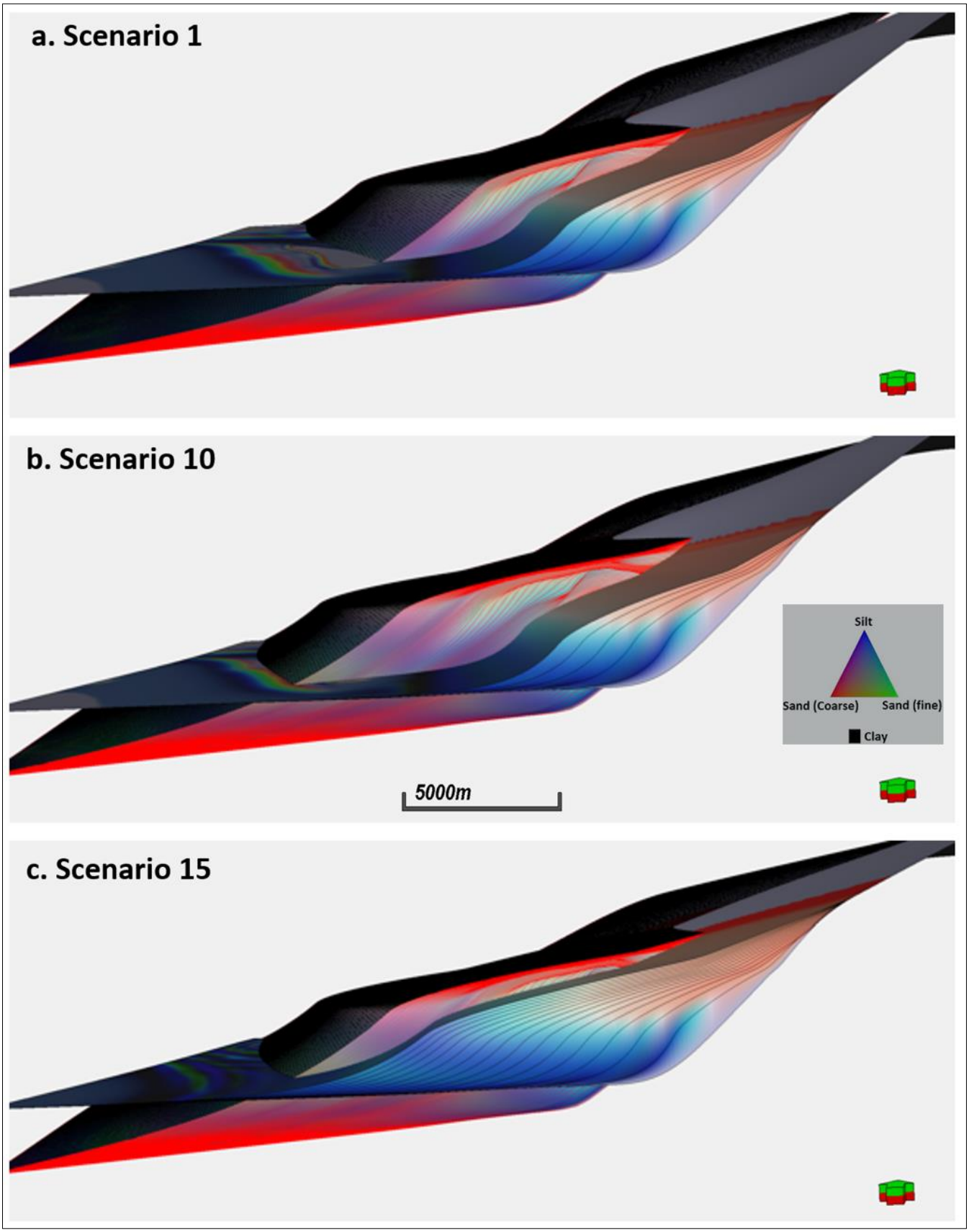

Fig 6. Stratigraphic simulation scenarios depicting sediment deposition in a shallow marine framework. **a.** scenario 1 involves equal proportions of sediment input, a relatively low subsidence rate and low water depth, **b.** scenario 10 uses high proportions of fine sand and silt (i.e. 70%) in the sediment mix, abrupt changes in subsidence rate, and a relatively high water depth, c. scenario 15 involves very high proportions of fine sand and silt (i.e. 80%), steady rate of subsidence and uplift in the sediment source area, and a relatively low water depth.

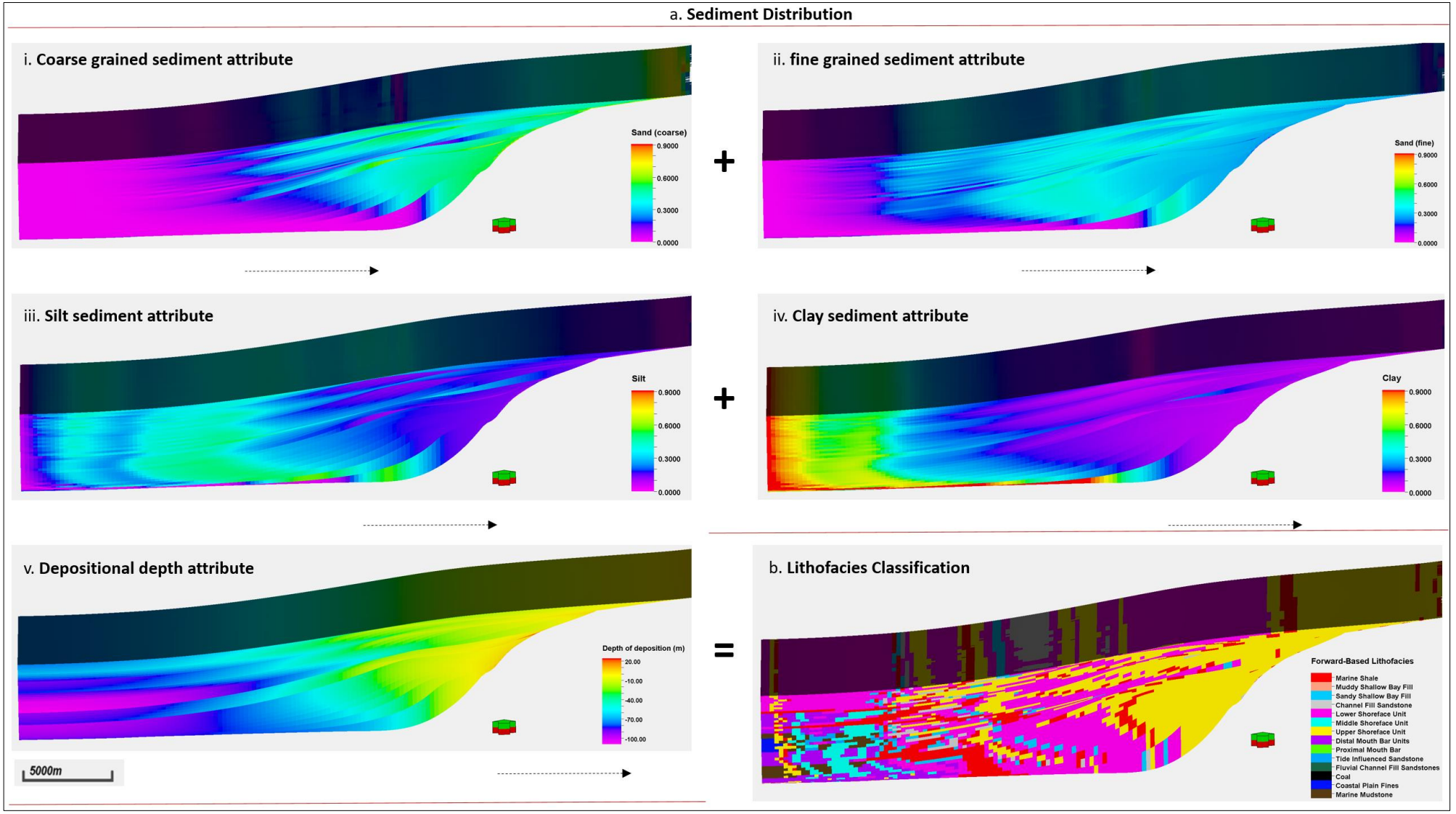

Fig 7 a. Sediment distribution patterns in the geological process modeling software. b. lithofacies classification using the property calculator tool in Petrel^{TM}.

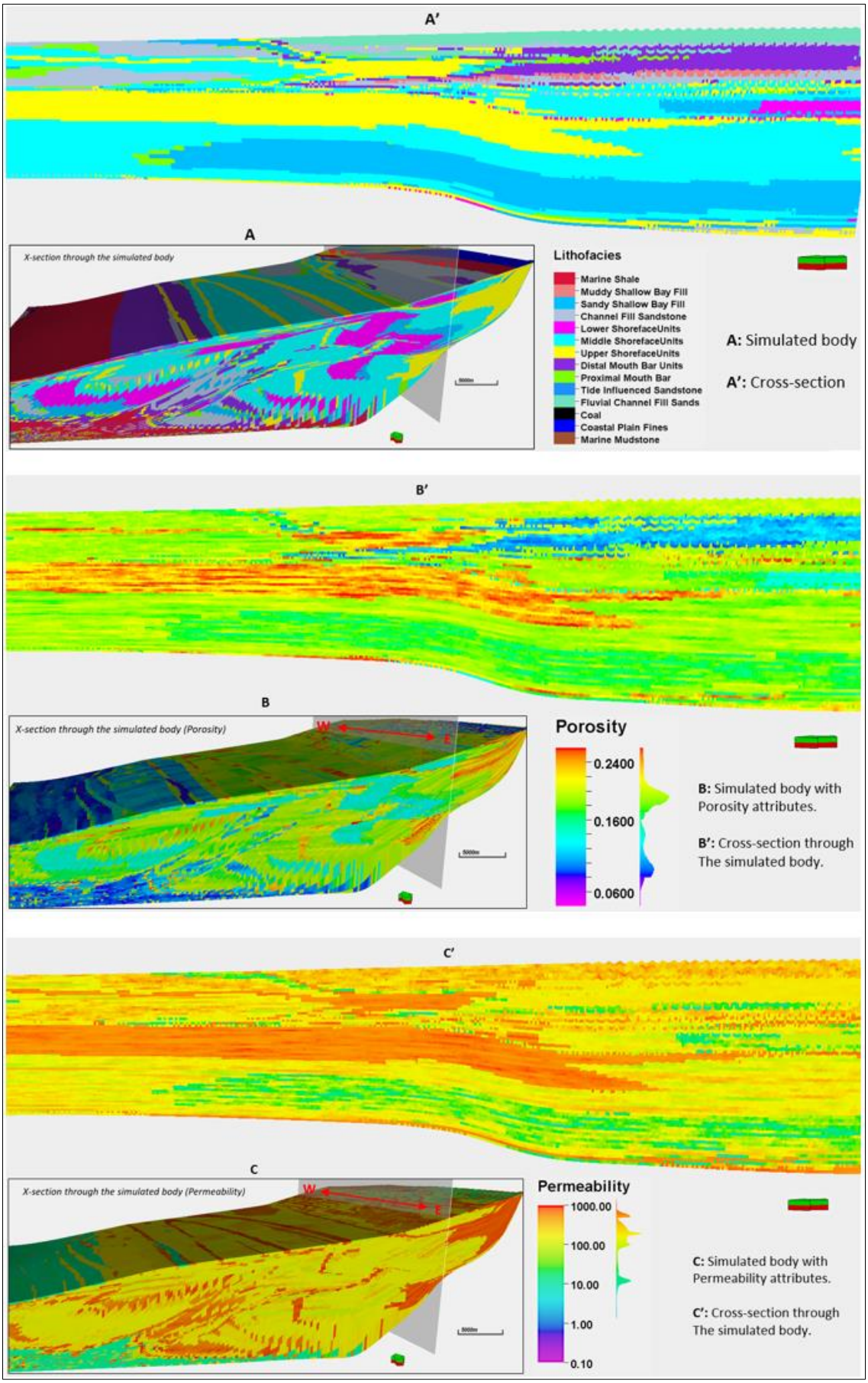

Fig 8. Property characterization in the stratigraphic using the property calculator tool in Petrel. Also showing a cross-sectional view through the model.

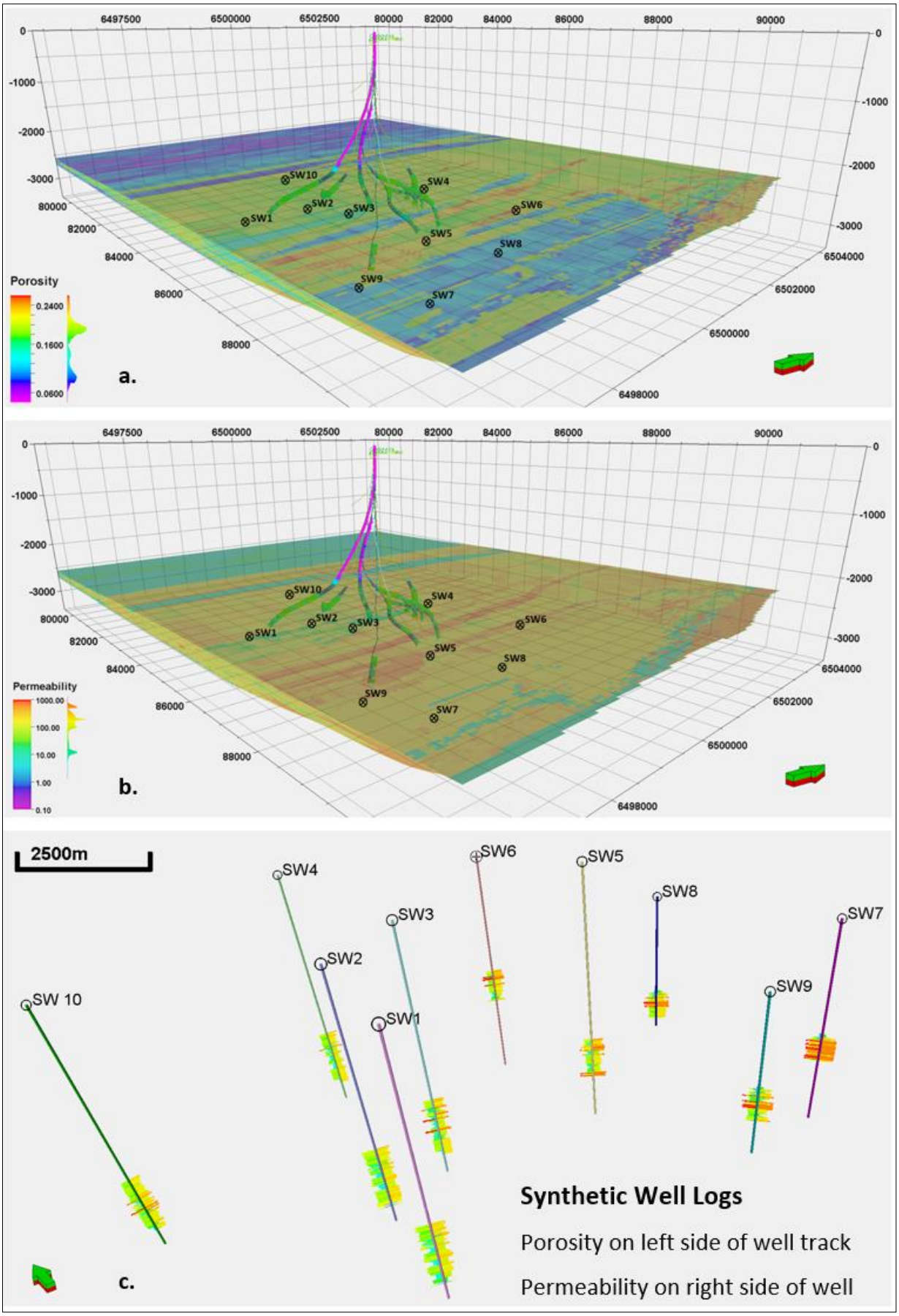

Fig 9. Synthetic wells derived from a forward stratigraphic-driven porosity and permeability models. The average distance between the synthetic wells shown in Figure 9c is about 0.9 km apart (maximum and minimum separation distance of 1.3 km and 0.65 km respectively).

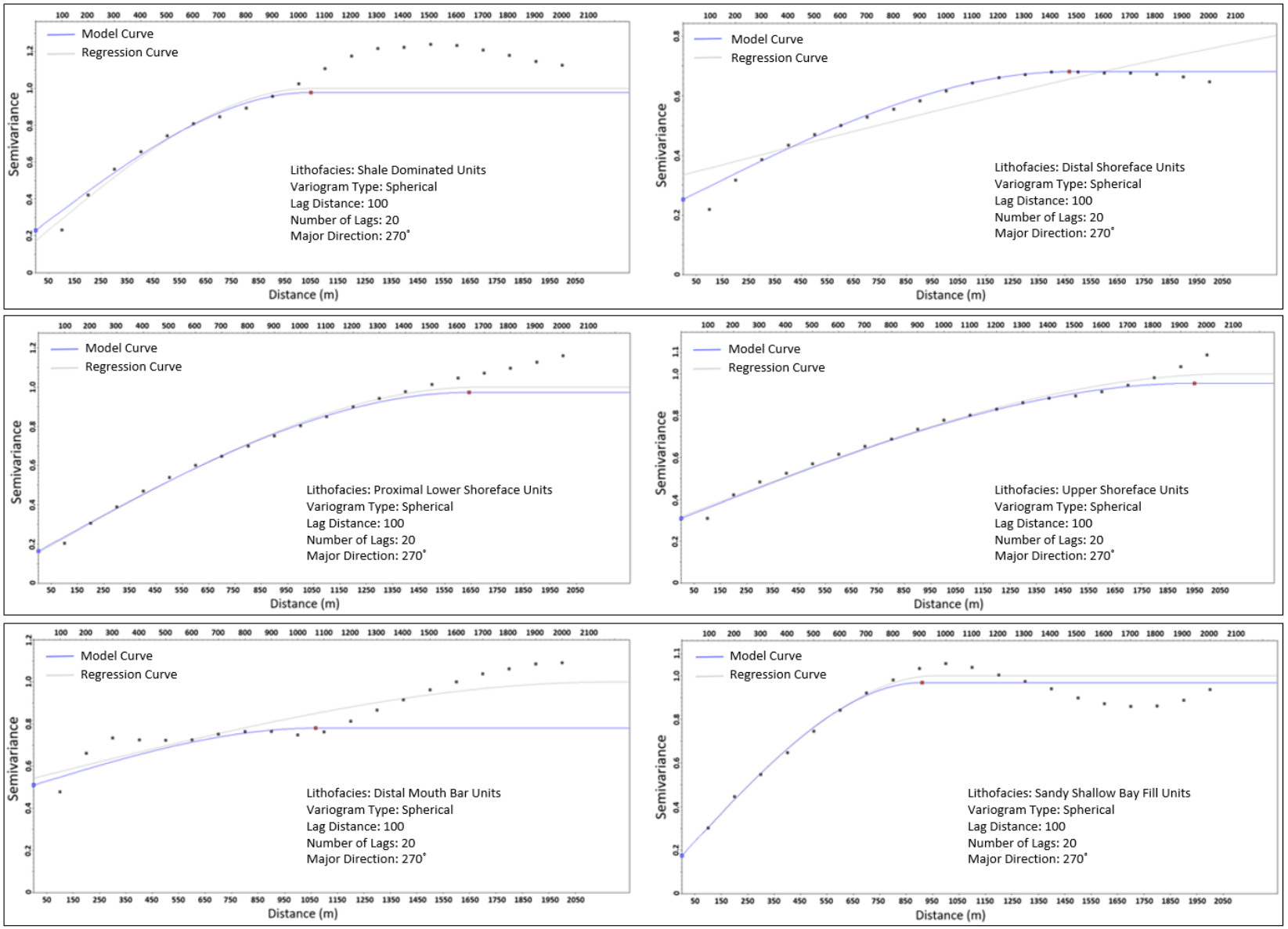

Fig 10. Variogram model of dominant lithofacies units extracted from the FSM. The points indicate the number of lags in the variogram. The distance between these lags is about 100 m. This figure shows the lags between sample pairs for calculating the variogram in the major direction (NE-SW) of the stratigraphic model.

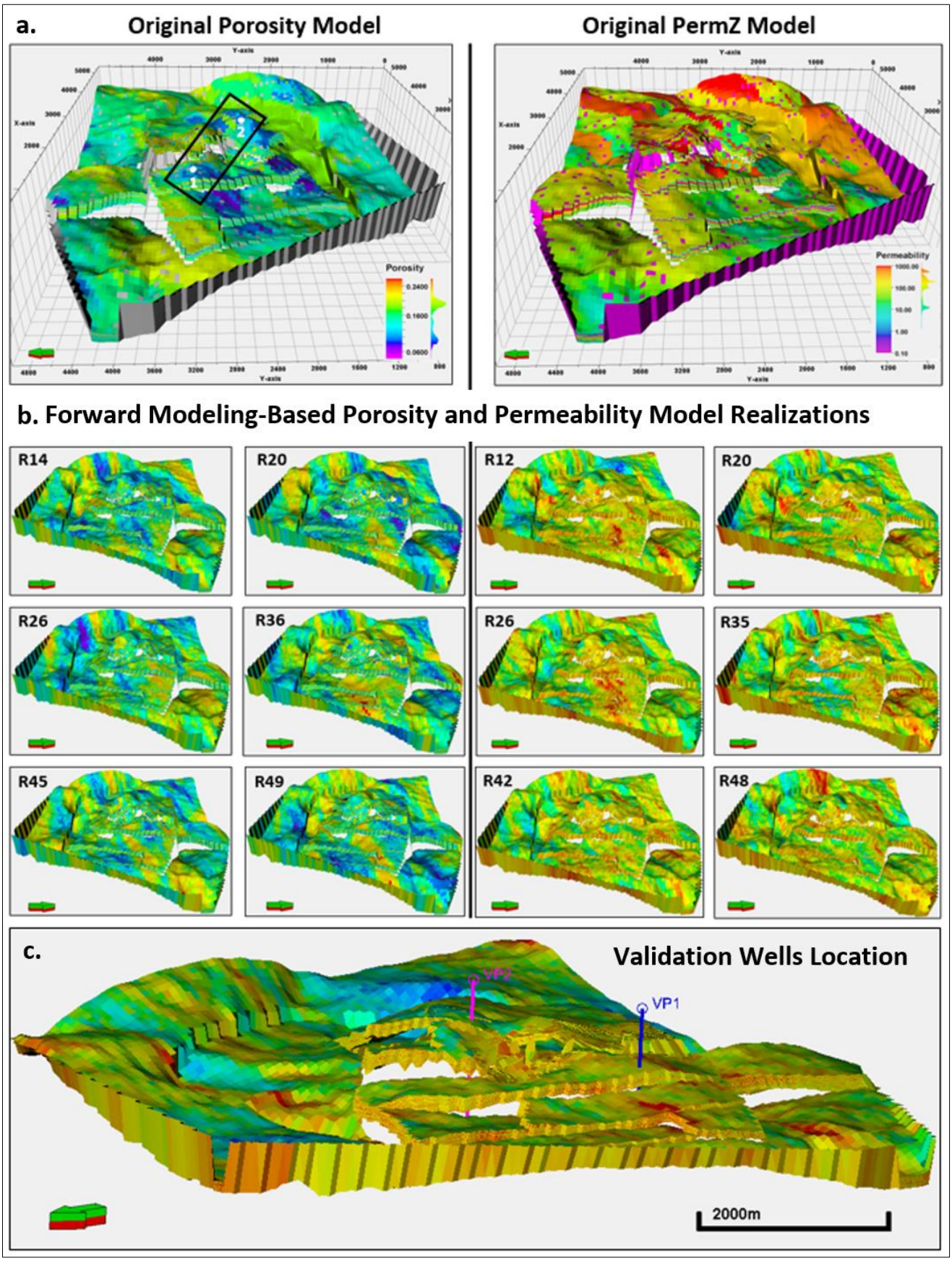

Fig 11. Comparing original Volve field model to the forward modeling-based models. Realizations 16, 20, 26, 36, 45, and 49 on the left half are porosity models, whilst realizations 12, 20, 26, 35, 42, and 48 on the right half show permeability models.

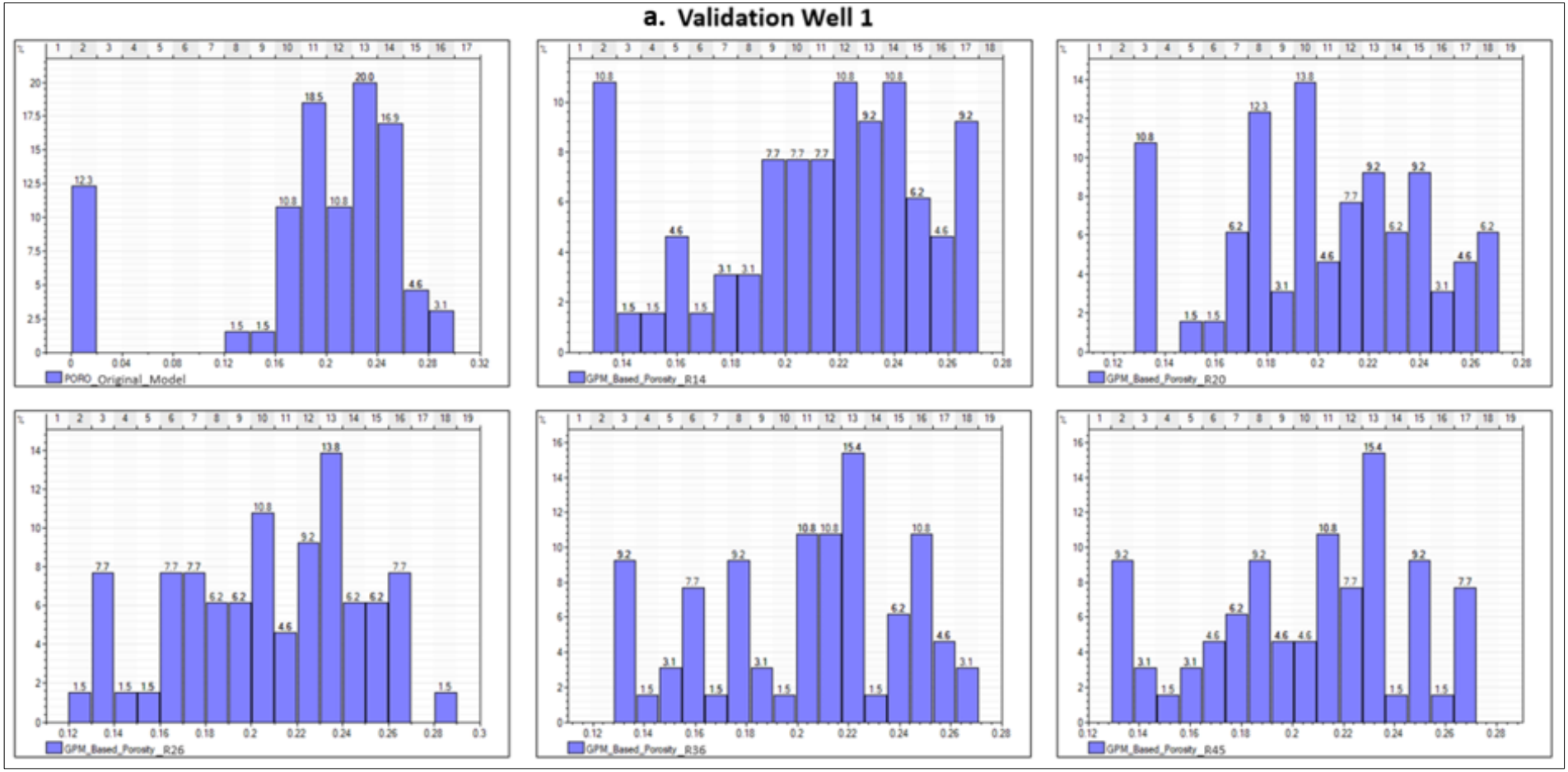

Figure 12a. Samples of validation Well 1 in five selected realizations , and how it compares to the samples at similar vertical interval in the original porosity and permeability models.

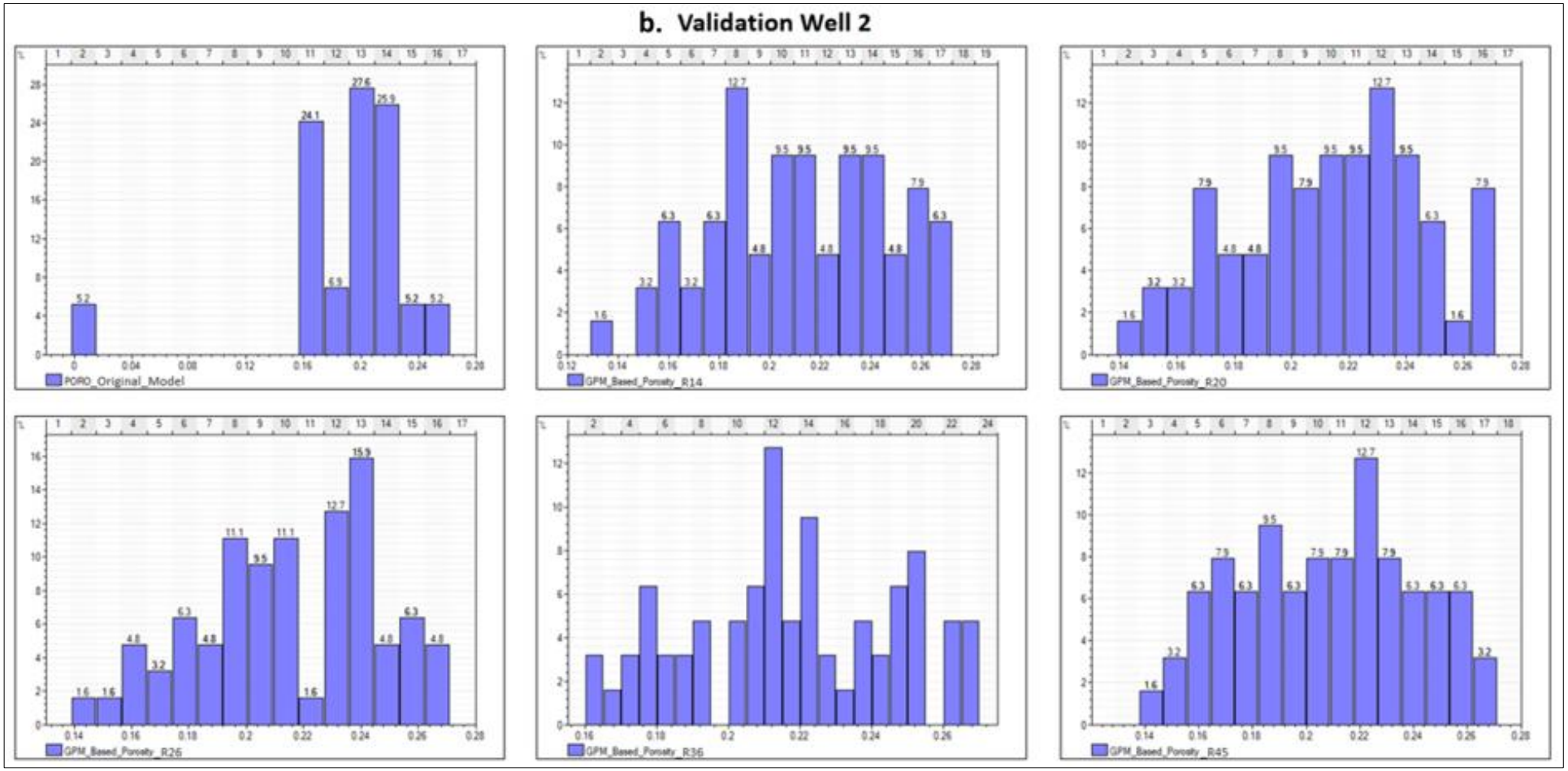

Figure 12b. Samples of validation Well 2 in five selected realizations , and how it compares to the samples at similar vertical interval in the original porosity and permeability models.

Table 1 Lithofacies-associations in the Hugin formation, Volve Field (after Kieft et al. 2011).

Code	Facies	Description	Thickness (t); extent (l)	Wireline-log Attribute	Interpretation
A	A1	Parallel-laminated mudstone with occasional siltstone inputs. Monospecific pattern of disorder bivalves parallel to bedding.	t= 30-425 cm l= 6 to 29 km	GR= 41-308 API DT= 225-355 μsm^{-1} NPHI= 0.17-0.45 v/v RHOB= 2280-2820 gcm^{-3}	Restricted marine shale
	A2	Interbedded claystone and very fine-grained sandstone; non-parallel and wavy lamination. Scarcely bivalve shells oriented parallel to bedding.	t= 10-725 cm l= 8 km to 13 km	GR= 71-65 API DT= 189-268 μsm^{-1} NPHI=? RHOB= 2280-2820 gcm^{-3}	Muddy Shallow bay-fill
	A3	Fine to medium grained sandstone; moderately to well sorted grains. Wavy bedding, cross bedding, rare wave ripples	t= 60-370 cm l <8 km	GR= 18-46 API DT= 199-314 μsm^{-1} NPHI= 0.07-0.52 v/v RHOB= 1690-2745 gcm^{-3}	Sandy shallow bay-fill
	A4	Coarse to fine-grained sandstones with alternating upward fining to coarsening trend. Moderately sorted grains. Sparse sedimentary structures.	t= 250-500 cm l= 1.8 km to 4.2 km	GR= 7-35 API DT= 175-230 μsm^{-1} NPHI= 0.038-0.146 v/v RHOB= 2280-2820 gcm^{-3}	Marine channel-fill sandstones
B	B1	Upward-coarsening siltstone to fine-grained moderate sorted sandstones, with shell debris, and quartz granules.	t= 30-480 cm l = <2 km	GR= 18-80 API DT= 168-291 μsm^{-1} NPHI= 0.038-0.191 v/v RHOB= 2322-2723 gcm^{-3}	Distal lower shoreface
	B2	Very fine-fine grained, moderate to well sorted sandstone. Fine grained carbonaceous laminae, typically low angle cross beds.	t= 130-440 cm l = 1.7 km – 8 km	GR= 20-56 API DT= 179-277 μsm^{-1} NPHI= 0.048-0.168 v/v RHOB= 2314-2696 gcm^{-3}	Proximal lower shoreface
	B3	Coarsening upward, cross laminated, fine to medium grained, well sorted sandstone; consist carbonaceous fragments	t= 425-800 cm l = 1.7 km – 8 km	GR= 15-25 API DT= 250-275 μsm^{-1} NPHI= 0.09-0.113 v/v RHOB= 2271-2342 gcm^{-3}	Upper Shoreface
C	C1	Highly bioturbated siltstone to very fine sandstones, which has beds of rounded granules	t= 175-1010 cm l = 7.2 km – 19.6 km	GR= 20-80 API DT= 230-260 μsm^{-1} NPHI= 0.08-0.169 v/v RHOB= 2327-2521 gcm^{-3}	Distal mouth bar
	C2	Very fine to fine grained sandstones; low angle cross-bedding.	t= 290-775 cm l = < 5 km	GR= 12-58 API DT= 167-397 μsm^{-1} NPHI= 0.05-0.595 v/v RHOB= 1612-2705 gcm^{-3}	Proximal mouth bar
D	D1	Fining upward coarse to fine grained sandstone; stacked fining upward beds with rare coarse grained stringers.	t= 740-820 cm l = < 2 km	GR= 8-134 API DT= 235-335 μsm^{-1} NPHI= 0.14-0.460 v/v RHOB= 2284-2570 gcm^{-3}	Tidally influenced fluvial channel fill sandstone
	D2	Fining upward coarse to medium grained sandstone. Carbonaceous laminae and fragments. Sharp, and cohesive contact at bed base	t= 580 cm l = < 2 km	GR= 9-34 API DT= 241-297 μsm^{-1} NPHI= 0.14-0.289 v/v RHOB= 2168-2447 gcm^{-3}	fluvial channel fill sandstone
E	E1	Coal and carbonaceous shale. Basal contact, typically parallel.	t= 30-520 cm l= 6 km to 19.6 km	GR= 8-56 API DT= 313-427 μsm^{-1} NPHI= 0.24-0.529 v/v RHOB= 1930-2225 gcm^{-3}	coal
	E2	Alternating dark grey mud/claystone and siltstone to very fine-grained sandstone. Wavy to non-parallel lamination.	t= 60 cm l = < 2 km	GR= 32-60 API DT= 358-415 μsm^{-1} NPHI= 0.43-0.49 v/v RHOB= 1994-2148 gcm^{-3}	Coastal plain fines

Table 2. Input parameters applied in running the simulations in GPM™

		Initial Conditions- GPM Input Parameters												
		Simulation Duration	Sediment Type Proportion (%)				Avg. Water Velocity	Avg. Sediment Velocity	Erodibility	Diffusion Coefficient	Avg. Sea Level	Turbidite Event Interval	Steady Flow Iteration	Sediment Movement
		(Ma– 0a) Years	Sand (Coarse)	Sand (Fine)	Silt	Clay	(m/a)	(m/a)			Interval (m)	(/years)	(/hrs)	Coefficient
GPM Scenarios (GS)	S1	0.02 – 0	25	25	25	25	0.11	0.03	0.35	0.11	30	2500	10	0.001
	S2	0.25 – 0	25	25	25	25	0.15	0.03	0.45	0.15	70	1000	15	0.012
	S3	0.5 – 0	25	25	25	25	0.11	0.02	0.55	0.11	120	1000	20	0.012
	S4	0.7 – 0.05	25	25	25	25	0.08	0.02	0.35	0.08	100	500	25	0.0011
	S5	1.5 – 0	15	35	30	20	0.15	0.04	0.50	0.15	80	5000	20	0.001
	S6	3.0 – 0	50	25	15	10	0.13	0.04	0.50	0.13	70	5000	30	0.0012
	S7	3.5 – 0	50	25	15	10	0.11	0.04	0.50	0.11	70	10000	15	0.001
	S8	4.0 – 0	50	25	15	10	0.13	0.04	0.50	0.13	90	5000	20	0.0015
	S9	4.5 – 0	15	45	25	15	0.1	0.02	0.45	0.1	50	10000	30	0.0012
	S10	5.0 – 0	15	45	25	15	0.12	0.02	0.45	0.12	55	10000	35	0.0013
	S11	5.5 - 0	15	45	25	15	0.12	0.02	0.45	0.12	40	5000	40	0.0013
	S12	6.0 – 0	15	45	25	15	0.1	0.02	0.45	0.1	60	10000	35	0.0011
	S13	6.5 – 0	10	25	55	10	0.13	0.03	0.48	0.13	100	20000	50	0.0010
	S14	7.0 – 0	10	25	55	10	0.16	0.03	0.48	0.16	40	20000	45	0.0011
	S15	7.5 – 0	10	25	55	10	0.13	0.03	0.48	0.13	40	20000	40	0.0012
	S16	8.0 – 0	10	25	55	10	0.15	0.03	0.48	0.15	30	10000	30	0.0010
	S17	8.5 – 0	10	25	45	20	0.14	0.02	0.45	0.14	50	50000	50	0.0010
	S18	9.0 – 0	30	30	18	22	0.13	0.02	0.52	0.13	60	25000	35	0.0012
	S19	9.5 – 0	30	40	12	18	0.12	0.02	0.55	0.12	55	25000	20	0.0013
	S20	10.0 - 0	30	42	18	10	0.11	0.01	0.40	0.11	50	5000	15	0.0011

	Sediment Property								
	Sediment Type	**Diameter**	**Density**	**Initial Porosity**	**Initial Permeability**	**Compacted Porosity**	**Compaction**	**Compacted Permeability**	**Erodibility**
	Coarse Grained Sand	1.0 mm	2.70 g/cm³	0.21 m³/m³	500 mD	0.25 m³/m³	5000 KPa	50 mD	0.6
	Fine Grained Sand	0.1 mm	2.70 g/cm³	0.3 m³/m³	100 mD	0.15 m³/m³	2500 KPa	5 mD	0.45
	Silt	0.01 mm	2.65 g/cm³	0.38 m³/m³	50 mD	0.12 m³/m³	1200 KPa	2 mD	0.3
	Clay	0.001 mm	2.65 g/cm³	0.48 m³/m³	5 mD	0.05 m³/m³	500 KPa	0.1 mD	0.15

Table 3. Lithofacies classification in the forward stratigraphic model; showing the command used in the property calculator tool in Petrel™.

Lithofacies Classification		
Facies Code	**Lithofacies**	**Command Used in Petrel's Property Calculator**
0	Marine Shale	If(Sand_fine>=0.19 And Sand_fine<=0.21 Or Silt>=0.19 And Silt<=0.2 Or Clay>=0.2 And Clay<=0.21 Or Depth_of_deposition>=-82 And Depth_of_deposition<=-78)
1	Muddy Shallow Bay Fill	If(Sand_fine>=0.36 And Sand_fine<=0.38 Or Silt>=0.18 And Silt<=0.2 Or Clay>0.18 And Clay<=0.19 Or Depth_of_deposition>=-30 And Depth_of_deposition<=-20)
2	Sandy Shallow Bay Fill	If(Sand_coarse>=0.65 And Sand_coarse<=0.73 Or Sand_fine>=0.18 And Sand_fine<=0.22 Or Silt>=0.18 And Silt<=0.2 Or Clay>=0.17 And Clay<=0.18 Or Depth_of_deposition>=-3 And Depth_of_deposition<=0)
3	Channel Fill Sandstone	If(Sand_coarse>=0.5 And Sand_coarse<=0.68 Or Sand_fine>=0.23 And Sand_fine<=0.25 Or Silt>=0.17 And Silt<=0.18 Or Depth_of_deposition>=0 And Depth_of_deposition<=2)
4	Lower Shoreface Units	If(Sand_coarse>=0.19 And Sand_coarse<=0.31 Or Sand_fine>=0.19 And Sand_fine<=0.24 Or Silt>=0.4 And Silt<=0.48 Or Clay>=0.19 And Clay<=0.31 Or Depth_of_deposition>=-83 And Depth_of_deposition<=50)
5	Middle Shoreface Units	If(Sand_coarse>=0.32 And Sand_coarse<=0.53 Or Sand_fine>=0.25 And Sand_fine<=0.32 Or Silt>=0.26 And Silt<=0.32 Or Clay>=0.19 And Clay<=0.21 Or Depth_of_deposition>=-38 And Depth_of_deposition<=-12)
6	Upper Shoreface Units	If(Sand_coarse>=0.53 And Sand_coarse<=0.72 Or Sand_fine>=0.28 And Sand_fine<=0.33 Or Silt>=0.16 And Silt<=0.21 Or Depth_of_deposition>=-10 And Depth_of_deposition<=6)
7	Distal Mouth Bar Units	If(Sand_fine>=0.23 And Sand_fine<=0.27 Or Silt>=0.38 And Silt<=0.43 Or Clay>=0.19 And Clay<=0.21 Or Depth_of_deposition>=-95 And Depth_of_deposition<=-80)
8	Proximal Mouth Bar Units	If(Sand_coarse>=0.53 And Sand_coarse<=0.71 Or Sand_fine>=0.27 And Sand_fine<=0.32 Or Silt>=0.16 And Silt<=0.21 Or Clay>=0.06 And Clay<=0.07 Or Depth_of_deposition>=-30 And Depth_of_deposition<=-27)
9	Tide Influenced Sandstones	If(Sand_coarse>=0.53 And Sand_coarse<=0.71 Or Sand_fine>=0.26 And Sand_fine<=0.31 Or Silt>=0.35 And Silt<=0.41 Or Depth_of_deposition>=-5 And Depth_of_deposition<=1)
10	Fluvial Channel Sandstones	If(Sand_coarse>=0.54 And Sand_coarse<=0.56 Or Sand_fine>=0.27 And Sand_fine<=0.29 Or Silt>=0.19 And Silt<=0.21 Or Depth_of_deposition>=-2 And Depth_of_deposition<=2)
11	Coal	Estimated as background attribute
12	Coastal plain fines	If(Silt>=0.31 And Silt<=0.43 Or Clay>=0.31 And Clay<=0.35 Or Depositional_depth>=-100 And Depositional_depth<=-40)
13	Marine Mudstone	If(Sand_fine>=0.36 And Sand_fine<=0.38 Or Silt>=0.4 And Silt<=0.52 Or Clay>=0.45 And Clay<=0.78 Or Depth_of_deposition>=-105 And Depth_of_deposition<=-90)

Table 4. Porosity and Permeability estimate in identified lithofacies packages.

Code	Lithofacies	Average NPHI	Density Porosity	Estimated Porosity	KLOGH (mD)
0	Marine Shale	0.17 - 0.45	0.1	0.08 - 0.11	10.02 - 16.1
1	Muddy Shallow Bay Fill	0.17 - 0.42	0.1	0.08 - 0.13	23.85 - 102.3
2	Sandy Shallow Bay Fill	0.07 - 0.52	0.25	0.16 - 0.25	100.0 - 398.7
3	Channel Fill Sandstone	0.04 - 0.15	0.30	0.18 - 0.22	400.01 - 889.7
4	Distal Lower Shoreface	0.04 - 0.19	0.29	0.1 - 0.23	120.5 - 170.3
5	Proximal Shoreface	0.05 - 0.17	0.31	0.17 - 0.24	80.2 - 412.5
6	Upper Shoreface Units	0.09 - 0.11	0.28	0.21 - 0.26	650.2 - 1023.7
7	Distal Mouth Bar Units	0.08 - 0.17	0.27	0.09 - 0.17	170.5 - 223.1
8	Proximal Mouth Bar	0.05 - 0.59	0.12	0.19 - 0.21	130.5 - 314.3
9	Tide Influenced SS	0.14 - 0.46	0.26	0.15 - 0.20	220.0 - 512.6
10	Fluvial Sandstones	0.14 - 0.29	0.21	0.19 - 0.21	180.5 - 691.8
11	Coal	0.24 - 0.53	0.05	0.001	0.001
12	Coastal Plain Fines	0.43 - 0.49	0.06	0.04 - 0.12	5.2 - 34.6
13	Marine Mudstone	0.16 - 0.42	0.1	0.08 - 0.10	6.0 - 15.2

Table 5. Comparison of a) porosity, and b) permeability estimates in original petrophysical model and forward modeling-based porosity and permeability models.

a. Validation Well Position 1							
	Porosity: GPM-Based Model					Porosity: Original Model	
	Depth (m)						
Models	5 m	10 m	15 m	25 m	35 m	Depth (m)	Average Porosity
R14	0.22	0.24	0.16	0.22	0.16	5	0.2
R20	0.16	0.19	0.26	0.18	0.15	10	0.25
R26	0.18	0.17	0.23	0.16	0.19	15	0.27
R36	0.22	0.21	0.19	0.22	0.21	25	0.16
R45	0.25	0.2	0.23	0.22	0.15	35	0.13
R49	0.21	0.17	0.22	0.17	0.18		
Validation Well Position 2							
	Porosity: GPM-Based Model					Porosity: Original Model	
	Depth (m)						
Models	5 m	10 m	15 m	25 m	35 m	Depth (m)	Average Porosity
R14	0.17	0.16	0.24	0.15	0.25	5	0.17
R20	0.21	0.22	0.2	0.21	0.23	10	0.21
R26	0.21	0.2	0.21	0.25	0.24	15	0.21
R36	0.2	0.22	0.21	0.21	0.19	25	0.17
R45	0.22	0.19	0.2	0.19	0.21	35	0.19
R49	0.26	0.24	0.23	0.16	0.21		

b. Validation Well Position 1							
	Permeability_Z (mD): GPM-Based Model					Permeability_Z: Original Model	
	Depth (m)						
Models	5 m	10 m	15 m	25 m	35 m	Depth (m)	Average Perm_Z
R14	163.95	312.38	69.84	310.16	508.2	5	352.74
R20	290.84	315.09	105.66	273.04	200.63	10	312.38
R26	375.92	203.81	166.23	189.92	348.12	15	201.08
R36	418.03	203.27	190.9	168.9	370.56	25	199.76
R45	337.6	412.67	199.66	156.71	305.92	35	508.2
R49	370.89	129.33	291.77	175.53	551.18		
Validation Well Position 2							
	Permeability_Z (mD): GPM-Based Model					Permeability_Z: Original Model	
	Depth (m)						
Models	5 m	10 m	15 m	25 m	35 m	Depth (m)	Average Perm_Z
R14	320.34	336.22	151.08	464.22	132.98	5	6.6
R20	122.66	209.15	161.3	230.58	208.48	10	883.6
R26	151.48	710.07	175.09	384.49	169.48	15	30.3
R36	184.74	344.99	157.08	420.15	136.14	25	496.99
R45	91.44	361.04	77.17	382.85	134.56	35	156.6
R49	134.01	721.73	137.42	636.48	290.06		